

# MsFEM for advection-dominated problems in heterogeneous media: Stabilization via nonconforming variants

R.A. Biezemans<sup>1,2</sup>, C. Le Bris<sup>1</sup>, F. Legoll<sup>1</sup>, and A. Lozinski<sup>3</sup>

<sup>1</sup>École Nationale des Ponts et Chaussées and Inria, MATHERIALS project-team,  
6 et 8 avenue Blaise Pascal, 77455 Marne-La-Vallée Cedex 2, France

<sup>2</sup>now at CEA Saclay, 91191 Gif-sur-Yvette, France

<sup>3</sup>Université de Franche-Comté, CNRS, LmB, 25000 Besançon, France

Draft of June 21, 2024

## Abstract

We study the numerical approximation of advection-diffusion equations with highly oscillatory coefficients and possibly dominant advection terms by means of the Multiscale Finite Element Method. The latter method is a now classical, finite element type method that performs a Galerkin approximation on a problem-dependent basis set, itself pre-computed in an offline stage. The approach is implemented here using basis functions that locally resolve both the diffusion and the advection terms. Variants with additional bubble functions and possibly weak inter-element continuity are proposed. Some theoretical arguments and a comprehensive set of numerical experiments allow to investigate and compare the stability and the accuracy of the approaches. The best approach constructed is shown to be adequate for both the diffusion- and advection-dominated regimes, and does not rely on an auxiliary stabilization parameter that would have to be properly adjusted.

## 1 Introduction

We consider in this article the numerical approximation of the advection-diffusion problem

$$\begin{cases} \mathcal{L}^\varepsilon u^\varepsilon = -\operatorname{div}(A^\varepsilon \nabla u^\varepsilon) + b \cdot \nabla u^\varepsilon = f & \text{in } \Omega, \\ u^\varepsilon = 0 & \text{on } \partial\Omega, \end{cases} \quad (1)$$

on a bounded domain  $\Omega \subset \mathbb{R}^d$ , using a specific category of finite element type methods, henceforth abbreviated as FEM, namely that of multiscale finite element methods (MsFEM).

The difficulty of the problem we consider is twofold. We are interested in the case of an advection field  $b$  that dominates the diffusive effects (and that we assume to be slowly-varying) *and* of a highly oscillatory diffusion coefficient  $A^\varepsilon$ . Separately capturing either of these phenomena by a numerical approximation is already challenging.

First, even when the coefficients of the equation are varying slowly, advection-dominated problems are known to possibly lead to spurious oscillations in the numerical approximation, which may propagate, if the mesh is too coarse, from a thin and steep boundary layer at the outflow to the

entire domain. In practically relevant applications, the use of a mesh fine enough to prevent these spurious effects may lead to a prohibitively computationally expensive discrete problem. Adapted numerical approaches that provide sufficiently accurate results already on a coarse mesh are thus required. The advection-dominated nature of the problem can be addressed using now classical stabilization techniques [19, 40, 41, 25, 30]. A general exposition of such techniques may be for instance found in the textbooks [60, 59]. Most of them in particular imply the introduction of a stabilization parameter, the value of which has been given extensive attention, e.g. in [43]. Besides the one-dimensional setting, no general optimal strategy for adjusting this parameter is however known theoretically.

Second, even in the absence of advection, it is well known that the strongly heterogeneous character of  $A^\varepsilon$  must be accurately discretized in order for the numerical solution to capture even the macroscopic behavior of the solution  $u^\varepsilon$ . Classical FEM require a sufficiently fine mesh, which again may lead to an expensive discrete problem. Numerous methods have therefore been introduced to capture the multiscale behaviour of  $A^\varepsilon$  adequately on a coarse mesh. One may mention the heterogeneous multiscale method [26, 1], the localized orthogonal decomposition [6, 54, 55], and the multiscale finite element method [36, 28, 46, 14]. The present work is focused on the latter approach. MsFEM originally developed for pure diffusion problems have indeed also been extended to advection-dominated problems in [2, 34, 49, 50, 53, 15].

Let us recall that MsFEM is a Galerkin approximation of the partial differential equation under consideration on a basis consisting of *pre-computed* basis functions *adapted* to the fine-scale properties of the differential operator  $\mathcal{L}^\varepsilon$  (rather than, as in classical FEM, on standard polynomial functions). The precomputation of these basis functions in an offline stage has a cost, but, overall, there is a significant computational gain if the global problem is to be solved multiple times (e.g. in design loops, optimization problems, uncertainty quantification, inverse problems, time-dependent problems, etc). In such cases, the adapted basis functions indeed have to be computed only once and the dimension of the global discrete problem is drastically reduced as compared to that of a direct approach put in action on a fine mesh. At the time of the introduction of the method in [36], it was proposed to only encode in these basis functions the differential operator of highest order of the equation. In the context of the specific advection-diffusion equation (1), where this operator is  $-\operatorname{div}(A^\varepsilon \nabla \cdot)$ , the corresponding variant of MsFEM was investigated in [49]. A classical SUPG stabilization technique was then employed to achieve the required stability in the advection-dominated regime. Another variant of MsFEM for (1), abbreviated as Adv-MsFEM here, relies on basis functions that *both* encode the advection and the diffusion coefficients of the equation. Such an MsFEM was first investigated in [57, 58] for both steady and unsteady problems, and then further studied in [49]. For the case of the *steady* advection-diffusion problem, a convergence analysis for this Adv-MsFEM variant was given in the one dimensional setting in [49], but the method was found to be unstable in higher dimensions. There is however not yet a general theoretical understanding of the stabilizing properties of this MsFEM variant. This motivates our present investigation. Let us also mention in passing the work [4], which combines the MsFEM proposed in [3] with the method of characteristics to obtain a stable approximation of unsteady advection-diffusion problems.

Our present work reveals the link between Adv-MsFEM and the classical residual-free bubble method of [18, 16, 31], which sheds new light on the stabilizing properties of Adv-MsFEM and enables us to explain its instability in dimensions higher than one. For higher-dimensional problems, we show by numerical evidence that a certain variant of Adv-MsFEM that uses a basis set composed of functions *weakly* continuous at the interfaces of the coarse mesh and bubbles only vanishing *weakly* on those interfaces provides a more effective stabilization than approaches enforcing continuity and/or vanishing by Dirichlet type conditions on the interfaces. The method thus constructed is

shown to perform adequately for both the diffusion and advection-dominated regimes and, moreover, does not involve any adjustable parameter as many stabilization approaches for classical FEM often do.

Our article is organized as follows. In Section 2, we first briefly recall FEM, classical stabilization techniques (Section 2.1) and MsFEM (Section 2.2). The reader familiar with either, or all, of these now classical notions may easily skip the corresponding sections and directly proceed to the sequel. In Section 2.3, we recall Adv-MsFEM (as in [57, 58, 49]) and provide some new insights into the stabilizing properties of this approach in the one-dimensional setting. We get to the heart of the matter with Section 3. We introduce there a variant of Adv-MsFEM with bubble functions and investigate it more closely in the one-dimensional setting. We explain in Section 3.2 why the observed stability results do not generalize to higher dimensional settings. In Section 4, we next introduce our most efficient approach, namely a (nonconforming) variant of Adv-MsFEM with *weak* bubbles, building up on the Crouzeix-Raviart MsFEM previously introduced in [48, 47]. In contrast to the (strong) bubbles considered in Section 3, which identically vanish at the boundary of the elements, these weak bubbles only vanish in an averaged sense. Both Galerkin and Petrov-Galerkin (with piecewise affine test functions) variants are considered. We collect in Table 1 below a glossary of the different MsFEM variants considered throughout the article. These methods are finally compared to one another numerically in Section 5. Two appendices, A and B, provide technical details on some mathematical arguments in the body of the text. In Appendix C, we eventually discuss the implementation of some of the methods in the spirit of the works [13, 12].

In short, the conclusions of this article are the following. We identify a portfolio of three approaches, the accuracy of which (outside the so-called boundary layer) is insensitive to the size of the advection: MsFEM-lin SUPG, Adv-MsFEM-CR-B and Adv-MsFEM-CR- $\beta$ , respectively defined by (18), (33) and (39). MsFEM-lin SUPG uses basis functions defined using only the diffusion part of the operator and satisfying affine boundary conditions. It includes an additional stabilization term. Adv-MsFEM-CR-B and Adv-MsFEM-CR- $\beta$  use basis functions defined using the complete operator and satisfying Crouzeix-Raviart type boundary conditions. They include no stabilization term. They involve (weak) bubble basis functions (also satisfying Crouzeix-Raviart type boundary conditions), which allow for a significant accuracy improvement while not increasing the size of the linear system to be solved, in view of a static condensation type observation. If the advection field is modified, then the basis functions of the latter two methods need to be recomputed. On the other hand, the latter two methods do not depend on the choice of a stabilization parameter, for which a correct value may be difficult to find when considering strongly heterogeneous media. They also provide an accurate approximation in the boundary layer, and one of them (the Adv-MsFEM-CR- $\beta$  method) is directly amenable to a non-intrusive implementation without any loss in accuracy.

We also note that, in the case of advection-dominated problems posed in perforated domains, the MsFEM method using (edge-based and bubble) basis functions defined using the complete operator and satisfying Crouzeix-Raviart type boundary conditions has been observed to perform very satisfactorily (see [50]).

We eventually wish to point out that we have considered oversampling variants, and Petrov-Galerkin variants using multiscale test functions that locally solve the adjoint problem rather than the direct problem (see Remarks 2.2 and 4.4). These variants have been observed to be less efficient (i.e., for an identical coarse mesh, either more expensive and providing a similar accuracy, or less accurate at equal computational cost) than the three methods mentioned above. We eventually note that we have purposely not considered Discontinuous Galerkin approaches, which in general require additional parameters, the value of which may be challenging to choose in the context of heterogeneous media.

Method	Operator used to define the basis functions	Boundary conditions for the local problems	Definition of the local problems	Global formulation
MsFEM-lin	Diffusion part only	affine	(16)	(17)
MsFEM-lin SUPG	Diffusion part only	affine	(16)	(18)
Adv-MsFEM-lin	Complete operator	affine	(19)	(21)
Adv-MsFEM-lin-B	Complete operator	affine	(19) and (25)	(27)
Adv-MsFEM-CR	Complete operator	Crouzeix-Raviart	(30)	(31)
Adv-MsFEM-CR-B	Complete operator	Crouzeix-Raviart	(30) and (32)	(33)
Adv-MsFEM-CR- $\beta$	Complete operator	Crouzeix-Raviart	(30) and (32)	(39)
PG Adv-MsFEM-CR	Complete operator	Crouzeix-Raviart	(30)	(40)
PG Adv-MsFEM-CR- $\beta$	Complete operator	Crouzeix-Raviart	(30) and (32)	(42)

Table 1: Glossary of the MsFEM variants

## 2 FEM discretization and related approaches

Our mathematical framework for the numerical approximation of (1) is the following.

In order to avoid technicalities related to the approximation of the boundary  $\partial\Omega$  of the domain, we assume that the domain  $\Omega$  is an open, bounded polytope (that is, a polygon in dimension 2, a polyhedron in dimension 3, etc). The diffusion tensor  $A^\varepsilon \in L^\infty(\Omega, \mathbb{R}^{d \times d})$  is assumed bounded and coercive, that is,

$$\text{for almost all } x \in \Omega, \quad \begin{cases} \forall \xi \in \mathbb{R}^d, & m |\xi|^2 \leq \xi \cdot A^\varepsilon(x) \xi, \\ \forall \xi_1, \xi_2 \in \mathbb{R}^d, & |\xi_2 \cdot A^\varepsilon(x) \xi_1| \leq M |\xi_2| |\xi_1|, \end{cases} \quad (2)$$

for some constants  $0 < m \leq M$  (independent of  $\varepsilon$ ). We recall that, in this work,  $A^\varepsilon$  is presumed highly oscillatory (the upperscript  $\varepsilon$  referring to the characteristic small length of oscillations). We shall make no further assumption (such as periodicity) on  $A^\varepsilon$  for the design of the numerical approaches in this article. We however mention in passing that the convergence proofs of MsFEM available to date in the literature all rely on a periodicity assumption (see e.g. [37, 3, 48, 51]).

We assume, say, that the advection field  $b \in L^\infty(\Omega, \mathbb{R}^d)$  satisfies

$$\operatorname{div} b = 0. \quad (3)$$

Under such assumptions, (1) has a unique solution in the Sobolev space  $H_0^1(\Omega)$ .

The variational (a.k.a. weak) formulation of (1) reads: find  $u^\varepsilon \in H_0^1(\Omega)$  such that

$$\forall v \in H_0^1(\Omega), \quad a^\varepsilon(u^\varepsilon, v) = F(v), \quad (4)$$

where, for all  $u, v \in H^1(\Omega)$ ,

$$a^\varepsilon(u, v) = \int_{\Omega} \nabla v \cdot A^\varepsilon \nabla u + v b \cdot \nabla u, \quad F(v) = \int_{\Omega} f v.$$

Under the above assumptions (2) and (3), it is classical to show that  $a^\varepsilon$  is coercive on  $H_0^1(\Omega)$ , such that a unique solution to (4) exists by the Lax-Milgram Theorem (see e.g. [59, Chapter 13]).

We next introduce a regular conforming triangular mesh  $\mathcal{T}_H$  of  $\Omega$  (made of triangles in dimension 2, tetrahedra in dimension 3, etc). The classical  $\mathbb{P}_1$  FEM relies on the approximation space

$$V_H = \{v \in \mathcal{C}(\Omega), \quad v|_K \in \mathbb{P}_1(K) \text{ for any } K \in \mathcal{T}_H \text{ and } v|_{\partial\Omega} = 0\},$$

that is, the finite-dimensional subspace of  $H_0^1(\Omega)$  consisting of all continuous functions that are piecewise affine and that vanish on the boundary. The  $\mathbb{P}_1$  FEM approximation of  $u^\varepsilon$  is the Galerkin approximation of  $u^\varepsilon$  on the space  $V_H$ , i.e., the unique element  $u_H \in V_H$  such that

$$\forall v_H \in V_H, \quad a^\varepsilon(u_H, v_H) = F(v_H). \quad (5)$$

Classically, this problem has a unique solution by the Lax-Milgram Theorem.

We are especially interested in (5) *in the advection-dominated regime*. In this case, both the size of the advection field and the heterogeneities of the diffusion tensor lead to multiscale effects that are challenging to capture numerically, as was mentioned in Section 1. We now successively briefly recall some classical techniques known to address these difficulties separately.

## 2.1 Methods for advection-dominated problems

### 2.1.1 Stabilization methods

In the single-scale case, *strongly consistent stabilization methods* consist in adding to the approximate variational formulation (5) the residue of the equation in each mesh element  $K \in \mathcal{T}_H$ , with a suitably adjusted stabilization parameter (denoted  $\tau$  below). The additional terms are chosen such that stronger stability properties hold for the numerical scheme, in particular in the streamline direction. We mention the Douglas-Wang method [25, 30], the Galerkin Least Squares method [40], and the Streamline Upwind/Petrov-Galerkin (SUPG) method [19]. We restrain our attention here to the latter variant. The  $\mathbb{P}_1$  SUPG method consists in finding  $u_H \in V_H$  such that

$$\forall v_H \in V_H, \quad a^\varepsilon(u_H, v_H) + a_{\text{stab}}(u_H, v_H) = F(v_H) + F_{\text{stab}}(v_H), \quad (6)$$

where  $a^\varepsilon$  (resp.  $F$ ) is the bilinear form (resp. linear form) within the classical variational formulation (4), and where, for all  $u_H, v_H \in V_H$ , we introduce the stabilization terms

$$a_{\text{stab}}(u_H, v_H) = \sum_{K \in \mathcal{T}_H} \int_K \tau (-\operatorname{div}(A^\varepsilon \nabla u_H) + b \cdot \nabla u_H) (b \cdot \nabla v_H), \quad (7)$$

$$F_{\text{stab}}(v_H) = \sum_{K \in \mathcal{T}_H} \int_K \tau f (b \cdot \nabla v_H). \quad (8)$$

When the sequence of matrices  $A^\varepsilon$  admits an homogenized limit  $A^*$ , the above strategy suggests to consider the stabilization formulation (6) with the bilinear form

$$a_{\text{stab}}(u_H, v_H) = \sum_{K \in \mathcal{T}_H} \int_K \tau (-\operatorname{div}(A^* \nabla u_H) + b \cdot \nabla u_H) (b \cdot \nabla v_H) \quad (9)$$

instead of (7). Since, in many practically relevant cases, this homogenized diffusion matrix  $A^*$  is (at least at the scale of each element  $K$  of our coarse mesh) constant and since all the second derivatives of a piecewise affine function vanish within each element, the form (9) also exactly reads

$$a_{\text{stab}}(u_H, v_H) = \sum_{K \in \mathcal{T}_H} \int_K \tau (b \cdot \nabla u_H) (b \cdot \nabla v_H). \quad (10)$$

Given that  $\mathbb{P}_1$  SUPG is considered in this work exclusively for the purpose of comparison and in the regime of small  $\varepsilon$ , we actually decide to take inspiration from the above case and adopt this

form (10) (together with (6) and (8)) in the general setting, even though, *strictly speaking*, we presumably commit a small error in doing so.

The stabilization parameter  $\tau$  that appears in the definitions (10) and (8) of the stabilization terms must be carefully adjusted. This is the topic of many research efforts, see [43] for a review of some motivations. Briefly speaking, in the advection-dominated regime and in the case of a constant coefficient problem, a suitable choice for  $\tau$  is of the order of  $\frac{\text{diam}(K)}{2b_K}$  in each mesh element  $K$ , where the real number  $b_K$  provides a characteristic size of  $b$  in  $K$ .

It was established in [8] that, for certain stabilized finite element formulations, the stabilization terms can be derived on the basis of a completely different perspective, that of *bubble functions*. We recall the link between the SUPG method and the so-called concept of residual-free bubbles in the next section.

### 2.1.2 The residual-free bubble method

We recall here the basics of methods using *residual-free bubbles* [32, 16, 17] and how this relates to stability (in this context, we also refer to [38, 39]). In such methods, the approximation space  $V_H$  is enriched by a space  $\mathcal{B}_H$  of some functions that vanish on all mesh interfaces (hence the name *bubble function*). It was observed in [22, 38] that a generic, problem-independent choice of bubble function space  $\mathcal{B}_H$  is not effective to increase the stability of the scheme. The residual-free bubble (RFB) method consists in a Galerkin approximation of (4) on the space  $V_H \oplus \mathcal{B}_H$ , where  $\mathcal{B}_H$  depends on the differential operator  $\mathcal{L}^\varepsilon$ . It is chosen such that the RFB approximation  $u_H + u_B \in V_H \oplus \mathcal{B}_H$  locally satisfies the differential equation, that is,  $\mathcal{L}^\varepsilon(u_H + u_B) = f$  in each mesh element, or

$$\forall K \in \mathcal{T}_H, \quad \mathcal{L}^\varepsilon u_B = -\mathcal{L}^\varepsilon u_H + f \quad \text{in } K.$$

Since the bubble component  $u_B$  of the solution vanishes on all  $\partial K$ , this equation completely defines  $u_B$  in terms of the coarse part  $u_H$  of the numerical approximation. The numerical scheme that defines  $u_H$  is then given by

$$\forall v_H \in V_H, \quad a^\varepsilon(u_H, v_H) + a^\varepsilon(u_B, v_H) = F(v_H). \quad (11)$$

When the diffusion coefficient is constant and equal to  $m \text{Id}$ , the advection field  $b$  is constant and the right-hand side  $f$  is piecewise constant, the bubble part  $u_B$  can easily be characterized in terms of  $u_H$  and, for each mesh element  $K$ , a single bubble function  $b_K \in H_0^1(K)$  that solves

$$-m \Delta b_K + b \cdot \nabla b_K = 1. \quad (12)$$

We indeed have  $u_B = (f - b \cdot \nabla u_H)|_K b_K$  in each element  $K$ . Then, as shown in [16, 18], the numerical scheme (11) is identical to the  $\mathbb{P}_1$  SUPG scheme (6) *precisely when* the stabilization parameter is given by

$$\forall K \in \mathcal{T}_H, \quad \tau^B = \frac{1}{|K|} \int_K b_K \quad \text{on } K. \quad (13)$$

In the one-dimensional case, the parameter  $\tau^B$  can easily be computed analytically and equals the unique value for which the SUPG method is known to provide a solution that is exact at the vertices of the mesh:

$$\tau^B = \frac{H}{2|b|} \left( \coth \text{Pe}_H - \frac{1}{\text{Pe}_H} \right) \quad \text{with} \quad \text{Pe}_H = \frac{|b|H}{2m}. \quad (14)$$

It then corresponds to the Il'in-Allen-Southwell scheme [5] (see also [21]). In dimensions higher than one, no such exactness results are known for either the SUPG or the RFB method. Numerical observations show that the parameter  $\tau^B$  given by (12)–(13) (which can be numerically computed) is in fact too small to achieve full stabilization of the SUPG method, as was shown in [18]. More direct generalizations of the expression for the ideal parameter of the one-dimensional setting provide the desired stabilizing effect (see [43]).

For the practical implementation of the RFB method, a *two-level* FEM was proposed in [31], which can also be applied to the case of non-constant coefficients. The bubble component  $u_B$  of the solution is in turn split in two different bubble components (which both vanish on the mesh interfaces) according to  $u_B = u_B^\varepsilon + u_B^f$ , where

$$\forall K \in \mathcal{T}_H, \quad \mathcal{L}^\varepsilon u_B^\varepsilon = -\mathcal{L}^\varepsilon u_H \quad \text{and} \quad \mathcal{L}^\varepsilon u_B^f = f \quad \text{in } K. \quad (15)$$

The two-level FEM first computes, in each mesh element separately, and by a suitable FEM, the bubble function  $u_B^f$  and the bubble functions  $u_B^{\varepsilon,i} \in H_0^1(K)$  solution to  $\mathcal{L}^\varepsilon u_B^{\varepsilon,i} = -\mathcal{L}^\varepsilon \phi_i^{\mathbb{P}^1}$  in  $K$ , where  $\{\phi_i^{\mathbb{P}^1}\}_i$  is the standard basis set of the space  $V_H$  to which  $u_H$  belongs. The global problem (11) can then be solved. This two-level FEM strategy bears similarities with MsFEM, for which we will see below that local problems are approximated numerically to resolve the fine scales of the differential operator. More precisely, the so-called numerical correctors that we introduce below (see (22)–(23) or (65)) play a role similar to  $u_B^\varepsilon$ , while the bubble functions (see (25) or (32)) play a role similar to  $u_B^f$  for some specific right-hand sides.

**Remark 2.1.** The analysis of [31] shows that the bubble  $u_B^\varepsilon$  allows to achieve partial stabilization of FEM (in the sense that it decreases the ratio of the continuity constant over the coercivity constant in (11)). The bubble  $u_B^f$  plays no part there: it only affects the consistency of the method (and therefore its accuracy), but not its stability.

## 2.2 The multiscale finite element method for problems with oscillatory coefficients

The *multiscale finite element method* (MsFEM) seeks a Galerkin approximation of (1) on a coarse mesh, but does so on a low-dimensional approximation space that is specifically *adapted* to the differential operator  $\mathcal{L}^\varepsilon$ . The underlying idea was first introduced in [7]. One expects (and this is indeed the case) that, by hopefully correctly encoding the multiscale features in the approximation space, an accurate finite element method is obtained even on a coarse mesh.

The original version of MsFEM was specifically proposed in [36] and uses multiscale basis functions that locally, inside each mesh element  $K \in \mathcal{T}_H$ , resolve the oscillations of the differential operator of highest order and satisfy affine boundary conditions on  $\partial K$ . We shall refer to it here as MsFEM-*lin*, the suffix *lin* originating from the affine boundary conditions. More precisely, let  $\phi_1^{\mathbb{P}^1}, \dots, \phi_N^{\mathbb{P}^1}$  denote the standard basis of  $V_H$  defined by  $\phi_i^{\mathbb{P}^1}(x_j) = \delta_{i,j}$  for all vertices  $x_j$  of the mesh  $\mathcal{T}_H$  that do not lie on the boundary  $\partial\Omega$  (where  $\delta_{i,j}$  denotes the Kronecker symbol). Then define, for  $1 \leq i \leq N$ , the multiscale basis function  $\phi_i^\varepsilon \in H_0^1(\Omega)$  by the boundary value problems

$$\forall K \in \mathcal{T}_H, \quad \begin{cases} -\operatorname{div}(A^\varepsilon \nabla \phi_i^\varepsilon) = 0 & \text{in } K, \\ \phi_i^\varepsilon = \phi_i^{\mathbb{P}^1} & \text{on } \partial K. \end{cases} \quad (16)$$

Note that  $\phi_i^\varepsilon$  indeed belongs to  $H_0^1(\Omega)$  because continuity is imposed on the interfaces of the mesh. Also note that  $\phi_i^\varepsilon$  has the same support as the corresponding  $\mathbb{P}_1$  basis function  $\phi_i^{\mathbb{P}^1}$ .

Introducing the multiscale approximation space  $V_H^\varepsilon = \text{Span}\{\phi_i^\varepsilon, 1 \leq i \leq N\}$ , MsFEM-lin is now defined as finding  $u_H^\varepsilon \in V_H^\varepsilon$  such that

$$\forall v_H^\varepsilon \in V_H^\varepsilon, \quad a^\varepsilon(u_H^\varepsilon, v_H^\varepsilon) = F(v_H^\varepsilon). \quad (17)$$

Practically, the multiscale basis functions  $\phi_i^\varepsilon$  have to be computed numerically. This requires another discretization, for instance by a  $\mathbb{P}_1$  FEM on a fine mesh of  $K$ , that resolves the microstructure. Note that all the problems (16) are localized and may therefore be solved by modest computational resources. Interestingly enough, this holds true even when a direct discretization of (1) cannot be solved. Moreover, the problems (16) on all  $K$  are independent and are thus amenable to parallel computing. These computations form the *offline stage*. The global problem (17) on the low-dimensional space  $V_H^\varepsilon$  is next solved in the *online stage*. The online stage is repeated each time the right-hand side changes (or, say, the boundary conditions on  $\partial\Omega$  change, a case which we do not further consider here for the sake of conciseness). However, the basis functions  $\phi_i^\varepsilon$  do not depend on the right-hand side, and the offline stage is therefore done once and for all.

One of the main drawbacks of MsFEM-lin is the fact that *affine* boundary conditions are imposed in the local problems (16), while the exact solution  $u^\varepsilon$  presumably oscillates wildly throughout the domain. The "ideal" boundary conditions, namely those given by the actual values of  $u^\varepsilon$  along the boundaries of the mesh elements, are of course unknown, while some choice of boundary conditions is definitely required to compute the multiscale basis functions. The further improvements of the MsFEM proposed after its first introduction can therefore be interpreted as a search for improved boundary conditions for the multiscale basis functions. Some options that we mention here are, respectively, the oversampling technique, which imposes the (affine) boundary conditions of (16) on the boundary of an *extended* domain around  $K$  (the so-called oversampling patch) and Crouzeix-Raviart type boundary conditions (see [48, 47]), to which we will return in Section 4. In the context of diffusion problems, oversampling was already proposed along with MsFEM-lin in [36]. For the Crouzeix-Raviart type boundary conditions, it was introduced in [12]. A hierarchical enrichment of the multiscale space has been considered in [27, 35, 20, 52].

### 2.3 On Adv-MsFEM-lin and its stability

In spite of the development of improved boundary conditions for MsFEM, it is easy to understand that all the MsFEM variants mentioned in the previous Section 2.2 cannot provide an accurate approximation of  $u^\varepsilon$  when applied to (1), especially in the advection-dominated regime.

Indeed, MsFEM-lin reduces to  $\mathbb{P}_1$  FEM in the particular case when  $A^\varepsilon$  is constant, and this method is well known to be unstable in the advection-dominated regime. This is precisely the reason why, in [49], MsFEM-lin was stabilized by application of the SUPG method. Introducing a stabilization parameter  $\tau$ , the stabilized formulation of (17) then reads: find  $u_H^{\varepsilon, \text{SUPG}}$  satisfying

$$\begin{aligned} \forall v_H^\varepsilon \in V_H^\varepsilon, \quad a^\varepsilon\left(u_H^{\varepsilon, \text{SUPG}}, v_H^\varepsilon\right) + \sum_{K \in \mathcal{T}_H} \int_K \tau \left(b \cdot \nabla u_H^{\varepsilon, \text{SUPG}}\right) (b \cdot \nabla v_H^\varepsilon) \\ = F(v_H^\varepsilon) + \sum_{K \in \mathcal{T}_H} \int_K \tau f(b \cdot \nabla v_H^\varepsilon). \end{aligned} \quad (18)$$

An alternative MsFEM approach for a stable approximation of advection-dominated problems was actually studied in [49] (see also [57, 58]). It is based on the multiscale basis functions  $\phi_i^{\varepsilon, \text{adv}}$



defined, for all  $1 \leq i \leq N$ , as the unique solutions in  $H_0^1(\Omega)$  to

$$\forall K \in \mathcal{T}_H, \quad \begin{cases} -\operatorname{div} \left( A^\varepsilon \nabla \phi_i^{\varepsilon, \text{adv}} \right) + b \cdot \nabla \phi_i^{\varepsilon, \text{adv}} = 0 & \text{in } K, \\ \phi_i^{\varepsilon, \text{adv}} = \phi_i^{\mathbb{P}^1} & \text{on } \partial K. \end{cases} \quad (19)$$

The multiscale approximation space is

$$V_H^{\varepsilon, \text{adv}} = \operatorname{Span} \left\{ \phi_i^{\varepsilon, \text{adv}}, 1 \leq i \leq N \right\}. \quad (20)$$

The restriction of (4) to the finite-dimensional space  $V_H^{\varepsilon, \text{adv}}$  is called *Adv-MsFEM-lin*: find  $u_H^{\varepsilon, \text{adv}} \in V_H^{\varepsilon, \text{adv}}$  such that

$$\forall v_H^{\varepsilon, \text{adv}} \in V_H^{\varepsilon, \text{adv}}, \quad a^\varepsilon \left( u_H^{\varepsilon, \text{adv}}, v_H^{\varepsilon, \text{adv}} \right) = F \left( v_H^{\varepsilon, \text{adv}} \right). \quad (21)$$

Since the possibly dominant advection term is encoded in the approximation space, one may hope that no additional stabilization terms are required in (21) for a stable approximation. This was found to be actually the case for one-dimensional problems in [49] (see also [11, Section 10.4]). An error estimate similar to that of the SUPG method was even provided. However, it was also observed in [49] by numerical experiments that instabilities survive in higher-dimensional settings. In the remainder of the present Section 2.3, we present some new insights into the stability of Adv-MsFEM-lin in the one-dimensional setting, but also into the instability of the method in higher dimensions.

**Remark 2.2.** One could think of applying the above-mentioned oversampling strategy to Adv-MsFEM-lin (and to the Crouzeix-Raviart variant, Adv-MsFEM-CR, which we will introduce later on in this article). We did investigate this pathway. The methods are considerably more expensive, their added value in terms of accuracy is, comparatively, poor and large numerical instabilities are observed in the advection-dominated regime. They are therefore not further reported on in this article, and we prefer to turn our attention to what will turn out to be more efficient techniques.

The following first, simple result establishes, in a very particular setting, the absence of spurious oscillations in the Adv-MsFEM-lin solution.

**Lemma 2.3.** *Consider the solution  $u^\varepsilon$  to (1) in the one-dimensional setting with non-homogeneous Dirichlet boundary conditions along with  $u_H^{\varepsilon, \text{adv}}$ , its Adv-MsFEM-lin approximation. Then, in the particular case when  $f = 0$  on the right-hand side of (1), the two functions agree, that is  $u_H^{\varepsilon, \text{adv}} = u^\varepsilon$ .*

We prove this result in Appendix A. A different proof can be found in [11, Theorem 10.4]. Anyhow, the proof critically relies on the fact that, for any function  $v \in H_0^1(\Omega)$ , it is possible to build an interpolant of  $v$  in  $V_H^{\varepsilon, \text{adv}}$  which coincides with  $v$  on all element boundaries. Therefore, it cannot be generalized to higher dimensions.

A second ingredient to understand the stabilizing properties of Adv-MsFEM-lin emerges from rewriting the multiscale basis functions as follows. As a matter of fact, and in contrast to Lemma 2.3, the analysis applies to any dimension. Following [13, 12], we introduce, on each mesh element  $K$  and for all  $\alpha = 1, \dots, d$ , the numerical corrector  $\chi_K^{\varepsilon, \text{adv}, \alpha} \in H_0^1(K)$  as the unique solution to

$$\mathcal{L}^\varepsilon \chi_K^{\varepsilon, \text{adv}, \alpha} = -\mathcal{L}^\varepsilon x^\alpha \quad \text{in } K, \quad \chi_K^{\varepsilon, \text{adv}, \alpha} = 0 \quad \text{on } \partial K, \quad (22)$$

where  $x^\alpha = x \cdot e_\alpha$  is the  $\alpha$ -th coordinate (and  $e_\alpha$  denotes the  $\alpha$ -th canonical unit vector of  $\mathbb{R}^d$ ). The terminology "corrector" arises from homogenization theory, and we refer the reader to e.g. [9, 14]

for the necessary background. We extend each numerical corrector by 0 to all of  $\Omega$ . Then, for all  $1 \leq i \leq N$ , the multiscale basis function  $\phi_i^{\varepsilon, \text{adv}}$  satisfies

$$\phi_i^{\varepsilon, \text{adv}} = \phi_i^{\mathbb{P}_1} + \sum_{K \in \mathcal{T}_H} \sum_{\alpha=1}^d \partial_\alpha \left( \phi_i^{\mathbb{P}_1} \Big|_K \right) \chi_K^{\varepsilon, \text{adv}, \alpha} =: \phi_i^{\mathbb{P}_1} + \psi_i^{\varepsilon, \text{adv}}. \quad (23)$$

Indeed, using that  $\nabla \phi_i^{\mathbb{P}_1}$  is piecewise constant and the definition of  $\chi_K^{\varepsilon, \text{adv}, \alpha}$ , we have that  $\mathcal{L}^\varepsilon \psi_i^{\varepsilon, \text{adv}} = -\mathcal{L}^\varepsilon \phi_i^{\mathbb{P}_1}$  inside each mesh element. Thus,  $\mathcal{L}^\varepsilon \left( \phi_i^{\mathbb{P}_1} + \psi_i^{\varepsilon, \text{adv}} \right) = 0$  in each mesh element and the identity (23) holds because (19) has a unique solution.

Repeating the above computation for the Adv-MsFEM-lin approximation  $u_H^{\varepsilon, \text{adv}}$  itself, it follows that there (actually uniquely) exists a function  $u_H^{\mathbb{P}_1} \in V_H$  such that  $u_H^{\varepsilon, \text{adv}} = u_H^{\mathbb{P}_1} + u_H^{\text{corr}}$ , where

$$u_H^{\text{corr}} = \sum_{K \in \mathcal{T}_H} \sum_{\alpha=1}^d \partial_\alpha \left( u_H^{\mathbb{P}_1} \Big|_K \right) \chi_K^{\varepsilon, \text{adv}, \alpha}.$$

The bubble function  $u_H^{\text{corr}}$  satisfies  $\mathcal{L}^\varepsilon u_H^{\text{corr}} = -\mathcal{L}^\varepsilon u_H^{\mathbb{P}_1}$  inside each mesh element. The relation between  $u_H^{\mathbb{P}_1}$  and  $u_H^{\text{corr}}$  here is thus exactly the same as the relation (15) between  $u_H$  and  $u_B^\varepsilon$  in the RFB method.

By analogy to the study of [31] (and as briefly recalled in Remark 2.1 above), the approximation space of Adv-MsFEM-lin thus incorporates the same additional stabilizing components (compared to the standard  $\mathbb{P}_1$  FEM) as the RFB method. In the constant coefficient case, the computations in Appendix B (see (61) there) show that the left-hand side of (21) can be rewritten as the left-hand side of the  $\mathbb{P}_1$  SUPG scheme for  $u_H^{\mathbb{P}_1}$  (a scheme related to the RFB method, as discussed in Section 2.1.2). Even though we do not have a similar analysis in the heterogeneous case, these observations are consistent with the fact that Adv-MsFEM-lin may be more stable than MsFEM-lin, and that the additional stabilizing effect is more pronounced in the one-dimensional case than in higher dimensions (because of a better value for the effective SUPG parameter). More precisely, we may expect (and this is indeed what we observe numerically on Figures 1 and 3) Adv-MsFEM-lin to be stable in dimension one, and we understand why, in higher dimensions, the Adv-MsFEM-lin method, although possibly more stable than MsFEM-lin, is not sufficiently stable, as observed in [49].

In spite of the stabilizing properties of Adv-MsFEM-lin we have just discussed, its accuracy is poor, as can be seen in purple on Figure 1 below. In order to improve on Adv-MsFEM-lin and our earlier work [49], we essentially devote the rest of the present work to introducing new ways to stabilize the numerical approach. To begin with, we consider in the next section an additional bubble space to enrich the approximation space.

### 3 Adv-MsFEM-lin with bubble functions

In order to illustrate our past and some of our upcoming developments of MsFEM type approaches for (1), let us consider the one-dimensional setting, and choose

$$a^\varepsilon(x) = \alpha \left( 2 + \cos \left( \frac{2\pi x}{\varepsilon} \right) \right) \quad (24)$$

as oscillatory coefficient in (1), for  $\alpha = 2^{-7}$  and  $\varepsilon = 2^{-5}$ . We further set  $b = 1$ ,  $f(x) = \sin^2(3\pi x)$ , and use  $H = 2^{-3}$ . All basis functions are computed by a  $\mathbb{P}_1$  FEM on a fine mesh of size  $h = 2^{-9}$ .

On this fine mesh, the microstructure is resolved and the  $\mathbb{P}_1$  FEM is stable (the local *Péclet number*  $\text{Pe}_h = (|b|h)/(2\alpha)$  is indeed much smaller than 1, see [59, Chapter 13] for instance; we also note that the local *Péclet number*  $\text{Pe}_H = (|b|H)/(2\alpha)$  on the coarse mesh is much larger than 1). Figure 1 below compares the profiles of the main methods we have already introduced, or are about to introduce in this work.

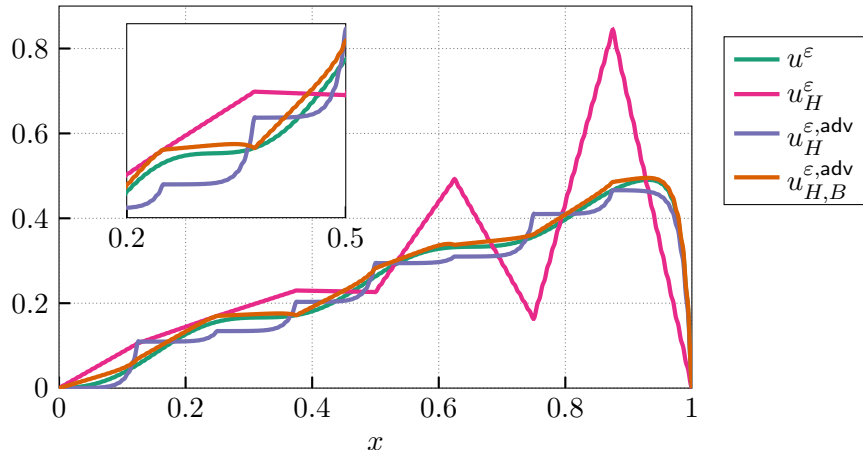


Figure 1: One-dimensional test case (24) with  $\alpha = 2^{-7}$ ,  $\varepsilon = 2^{-5}$ ,  $b = 1$  and  $H = 2^{-3}$ : comparison of the profiles of the exact solution  $u^\varepsilon$  to (1) (green curve) and its approximation by, respectively, MsFEM-lin ( $u_H^\varepsilon$  defined by (17); pink curve), Adv-MsFEM-lin ( $u_H^{\varepsilon,\text{adv}}$  defined by (21); purple curve) and Adv-MsFEM-lin-B ( $u_{H,B}^{\varepsilon,\text{adv}}$  defined by (27) below; orange curve). The purple curve in the close-up view in particular shows that the Adv-MsFEM-lin basis functions are close to step functions on each mesh element.

It is clear that the MsFEM-lin (pink curve) approximation  $u_H^\varepsilon$  is unstable: it shows spurious oscillations in the whole domain  $\Omega$ . On the contrary, we can observe the stability of Adv-MsFEM-lin (in purple). Although the exactness property of Lemma 2.3 is not satisfied here for Adv-MsFEM-lin (recall that  $f \neq 0$  in our numerical test), no spurious oscillation shows up for Adv-MsFEM-lin.

One clear disadvantage of Adv-MsFEM-lin is however visible in the close-up view of Figure 1: the basis functions  $\phi_i^{\varepsilon,\text{adv}}$  are heavily deformed by the advection field (in the absence of advection, they would resemble the standard piecewise affine functions  $\phi_i^{\mathbb{P}_1}$ , up to small oscillations). In combination with the boundary conditions imposed in the local problems (19), the advection field produces basis functions being close to step functions and having sharp boundary layers on each element. In contrast, the exact solution varies smoothly and only shows, as expected, a boundary layer near the outflow at  $x = 1$ . In spite of its stability, Adv-MsFEM-lin is unable to provide an accurate approximation of the exact solution  $u^\varepsilon$  to (1).

We now propose to enrich the multiscale approximation space  $V_H^{\varepsilon,\text{adv}}$  by an additional bubble that plays a role similar to that of  $u_B^f$  defined in (15) as the solution to  $\mathcal{L}^\varepsilon u_B^f = f$ , but is different from  $u_B^f$ . The difficulty with the bubble function  $u_B^f$  is indeed that the function contradicts a "dogma" of MsFEM since it depends on the right-hand side  $f$  and consequently cannot be pre-computed in an offline stage where  $f$  is (still) unknown. Instead, we introduce one bubble per mesh element that is *independent* of  $f$  and thus allows for the construction of an approximation space that can be computed once and for all in the offline stage. This new bubble, although strictly speaking different from  $u_B^f$ , however agrees with it (up to a multiplicative factor) when  $f$  is constant

throughout each coarse element. Intuitively, this slow variation of the right-hand side  $f$  is a perfectly decent assumption and our substitution is therefore rightful.

More precisely, for any  $K \in \mathcal{T}_H$ , we define the bubble function  $B_K^{\varepsilon, \text{adv}} \in H_0^1(K)$  as the unique solution to

$$\mathcal{L}^\varepsilon B_K^{\varepsilon, \text{adv}} = 1 \quad \text{in } K, \quad B_K^{\varepsilon, \text{adv}} = 0 \quad \text{on } \partial K, \quad (25)$$

and extend it by 0 outside  $K$ . Equivalently, setting  $\mathcal{B}_H = \bigoplus_{K \in \mathcal{T}_H} H_0^1(K)$ , the bubble  $B_K^{\varepsilon, \text{adv}}$  is the unique solution in  $\mathcal{B}_H$  to

$$\forall v \in \mathcal{B}_H, \quad a^\varepsilon \left( B_K^{\varepsilon, \text{adv}}, v \right) = \int_K v. \quad (26)$$

We next define the space  $V_{H,B}^{\varepsilon, \text{adv}} = V_H^{\varepsilon, \text{adv}} \bigoplus_{K \in \mathcal{T}_H} \text{Span} \left\{ B_K^{\varepsilon, \text{adv}} \right\}$ , and the Adv-MsFEM-lin method with bubbles (henceforth abbreviated Adv-MsFEM-lin-B): find  $u_{H,B}^{\varepsilon, \text{adv}} \in V_{H,B}^{\varepsilon, \text{adv}}$  such that

$$\forall v_{H,B}^{\varepsilon, \text{adv}} \in V_{H,B}^{\varepsilon, \text{adv}}, \quad a^\varepsilon \left( u_{H,B}^{\varepsilon, \text{adv}}, v_{H,B}^{\varepsilon, \text{adv}} \right) = F \left( v_{H,B}^{\varepsilon, \text{adv}} \right). \quad (27)$$

The typical profile of the bubble functions, in the one-dimensional constant coefficient case, is shown on Figure 2. We observe that these bubbles  $B_K^{\varepsilon, \text{adv}}$  also have a sharp boundary layer, just as the basis functions  $\phi_i^{\varepsilon, \text{adv}}$ , but that the layers of the two functions compensate. There thus exists an adequate linear combination of the functions  $\{\phi_i^{\varepsilon, \text{adv}}\}_i$  and  $\{B_K^{\varepsilon, \text{adv}}\}_K$  that resembles (up to small oscillations) the standard piecewise affine functions  $\phi_i^{\mathbb{P}^1}$ . We may thus expect (and this is indeed the case) the best approximation error of Adv-MsFEM-lin-B to be much smaller than that of Adv-MsFEM-lin.

An example of an Adv-MsFEM-lin-B approximation can be seen on Figure 1 in orange. Its accuracy is indeed much better than that of the Adv-MsFEM-lin approximation shown in purple. The computation of the multiscale space  $V_{H,B}^{\varepsilon, \text{adv}}$  requires one additional computation per mesh element in the offline stage of the MsFEM with respect to Adv-MsFEM in order to compute the additional bubble functions  $B_K^{\varepsilon, \text{adv}}$ .

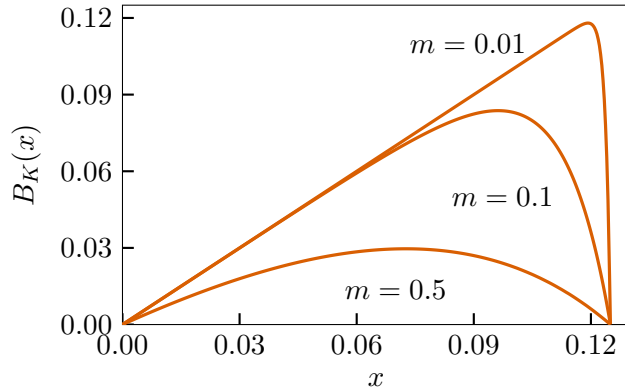


Figure 2: Profiles of the bubble functions  $B_K$  in the one-dimensional domain  $(0, 0.125)$  solving  $-m B_K'' + B_K' = 1$  (with homogeneous Dirichlet boundary conditions), for different values of  $m$ .

We notice that an alternative MsFEM enriched with bubble functions was already proposed in [61]. Our MsFEM strategy differs in at least two ways. First, as emphasized above, our bubble functions are independent of the right-hand side  $f$ . Second, our method is one-shot, whereas the method of [61] is an iterative procedure aimed at finding improved boundary conditions for

the bubble functions. For both reasons, our method abides by the two "dogmas" (and, more importantly, reproduces the simplicity and efficiency) of MsFEM when the basis functions are precomputed and no iteration is performed. This is in sharp contrast with approaches inspired by domain decomposition methods and relying on a different paradigm.

Lemma 3.1 below states an exactness property for Adv-MsFEM-lin-B in the one-dimensional setting. This shows that, in this setting, Adv-MsFEM-lin-B is stable when the right-hand side is piecewise constant. Figure 1 also shows numerically (and Figure 3 will later confirm this) that Adv-MsFEM-lin-B also provides a stable approximation for generic right-hand sides, again in the one-dimensional setting.

**Lemma 3.1.** *In the one dimensional setting and when  $f$  is piecewise constant on the coarse mesh, Adv-MsFEM-lin-B is exact.*

The proof of Lemma 3.1 is postponed until Appendix A, and we only consider there the case of homogeneous Dirichlet boundary conditions as in (1). The result of Lemma 3.1 actually also holds true for non homogeneous Dirichlet boundary conditions.

### 3.1 Further numerical comparisons in the one-dimensional setting

We now proceed further with our numerical comparisons of the methods in the one-dimensional setting. Although this setting may look like an oversimplified situation, we will draw some conclusions that are important for, and carry over to the more challenging two-dimensional situation addressed in Section 5.

We take the same test-case as above in (24), but now choose a faster oscillation  $\varepsilon = 2^{-8}$ , and, correspondingly, a smaller coarse mesh size  $H = 2^{-6}$  for MsFEM. For the fine mesh, on which the reference solution (denoted  $u_h^\varepsilon$ ) and the multiscale basis functions are computed, we take  $h = 2^{-5} \min\{\varepsilon, \alpha\}$ , so that, as above, the microstructure is resolved and the  $\mathbb{P}_1$  FEM is stable on the fine mesh (the local Péclet number  $\text{Pe}_h = (|b|h)/(2\alpha)$  is again much smaller than 1). For MsFEM-lin SUPG, and as suggested in [49], the stabilization parameter is

$$\tau = \frac{H}{2|b|} \left( \coth \text{Pe}_H - \frac{1}{\text{Pe}_H} \right) \quad \text{with} \quad \text{Pe}_H = \frac{|b|H}{2\alpha},$$

which coincides with the ideal value (13) for the  $\mathbb{P}_1$  SUPG method in the one-dimensional setting, for a constant diffusion coefficient equal to  $\alpha$  (see (14)). We are going to observe the quality of the results in function of the parameter  $\alpha$  within (24), which, given the formula of the Péclet number above, effectively measures the relative effect of advection versus diffusion.

On Figure 3, we aim to distinguish between unstable methods, which develop spurious oscillations propagating from the boundary layer at  $x = 1$  for small values of  $\alpha$ , and stable methods. Therefore, we start by measuring the error deliberately *excluding* the mesh element where the boundary layer lies, i.e., on  $\Omega_{\text{OBLE}} = (0, 1 - H)$  (the acronym OBLE standing for 'outside the boundary layer element'). The errors are normalized with respect to the norm of the reference solution  $u_h^\varepsilon$  on the same domain  $\Omega_{\text{OBLE}}$ . We shall further comment on this in Section 5.1.2 below, when we address the two-dimensional context (see Remark 5.1). This yields the left plot of Figure 3. On that figure, in addition to the methods discussed above, we also consider the PG Adv-MsFEM-CR- $\beta$  method: it is a Petrov-Galerkin method (where the test space is the  $\mathbb{P}_1$  space  $V_H$ ), where the trial space includes bubbles, where all basis functions (including the bubbles) are defined using the complete operator, and where the values of bubble degrees of freedom are approximated using a static condensation procedure (this method is defined by (42) below; note that, in the one-dimensional

case considered here, imposing Crouzeix-Raviart boundary conditions as in (42) simply consists in imposing the nodal values).

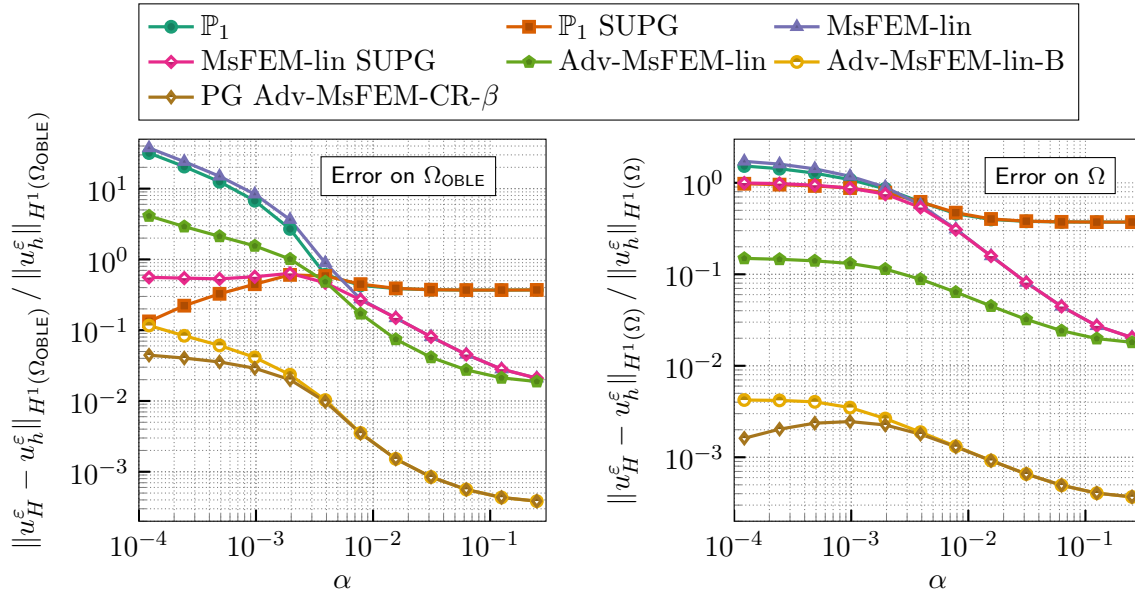


Figure 3: Relative errors (left: outside the boundary layer element; right: on the entire domain) between the reference solution  $u_h^\varepsilon$  and its various numerical approximations  $u_H^\varepsilon$ , for the one-dimensional test case (24), with  $b = 1$ ,  $\varepsilon = 2^{-8}$ ,  $H = 2^{-6}$  and different values of  $\alpha$ . In the diffusion-dominated regime,  $\mathbb{P}_1$  and  $\mathbb{P}_1$  SUPG on the one hand, as well as MsFEM-lin and MsFEM-lin SUPG on the other hand, yield almost identical results and the curves visually overlap.

The results of the left plot of Figure 3 confirm that  $\mathbb{P}_1$  and MsFEM-lin are not stable, since they suffer from spurious oscillations due to which the error explodes even when measured on  $\Omega_{\text{OBLE}}$ . The  $\mathbb{P}_1$  and  $\mathbb{P}_1$  SUPG methods, as well as MsFEM-lin and MsFEM-lin SUPG, yield almost identical results in the diffusion-dominated regime. This is natural because no stabilization is required in that regime, and in fact the stabilization parameter  $\tau$  is negligible here. The point where stabilization starts to matter can be used as an indication of when the advection starts to dominate. We discuss this further in Section 5.1.3.

The stable methods are  $\mathbb{P}_1$  SUPG, MsFEM-lin SUPG, Adv-MsFEM-lin-B, PG Adv-MsFEM-lin- $\beta$  and Adv-MsFEM-lin, although the latter, Adv-MsFEM-lin, is not accurate in the advection-dominated regime. This fact was anticipated above as a result of the shape of the basis functions  $\phi_i^{\varepsilon, \text{adv}}$  under the influence of a strong advection field (recall Figure 1). The error of  $\mathbb{P}_1$  SUPG is larger than that of the multiscale methods by one order of magnitude in the diffusion-dominated regime, as can be expected from the fact that  $a^\varepsilon$  is highly oscillatory with 4 periods per coarse mesh element ( $H = 4\varepsilon$ ).

On the other hand, we observe in the advection-dominated regime that the accuracy of  $\mathbb{P}_1$  SUPG method is comparable to Adv-MsFEM-lin-B, and that it even performs better than MsFEM-lin SUPG. This confirms the earlier findings of [49], noticing that the multiscale character of the diffusion is overshadowed by the advective effects when those dominate the diffusive effects. A more intuitive understanding of this phenomenon is provided by Figure 4, which shows the derivative of the reference solution  $u_h^\varepsilon$  and several numerical approximations on a coarse mesh. The two cases shown correspond to the values  $\alpha = 2^{-9} \approx 2 \times 10^{-3}$  and  $\alpha = 2^{-13} \approx 10^{-4}$  on Figure 3, the latter being the smallest value considered on that figure.

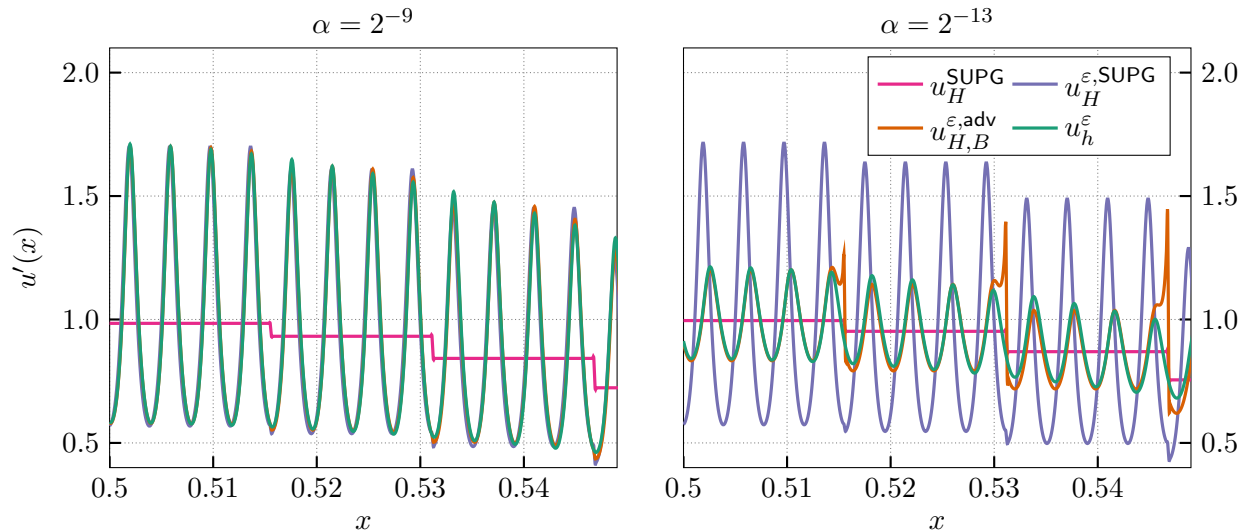


Figure 4: One-dimensional test case (24) with  $b = 1$ ,  $\varepsilon = 2^{-8}$  and  $H = 2^{-6}$ : fine-scale oscillations of the derivative of the reference solution  $u_h^\varepsilon$  and three stable (Ms)FEM approximations ( $\mathbb{P}_1$  SUPG, MsFEM-lin SUPG and Adv-MsFEM-lin-B), for two values of the diffusion strength  $\alpha$  (note that the horizontal and vertical scales are identical on both figures). The  $\mathbb{P}_1$  SUPG approximation is denoted by  $u_H^{\text{SUPG}}$ . For  $\alpha = 2^{-9}$ , the MsFEM-lin SUPG approximation  $u_H^{\varepsilon, \text{SUPG}}$  and the Adv-MsFEM-lin-B approximation  $u_{H,B}^{\varepsilon, \text{adv}}$  visually coincide with  $u_h^\varepsilon$  at the scale of the plot. For  $\alpha = 2^{-13}$ , only  $u_{H,B}^{\varepsilon, \text{adv}}$  captures the oscillations of  $u_h^\varepsilon$  correctly (except close the boundary of mesh elements).

It is clear from Figure 4 that the amplitude of the oscillations of the derivative of  $u_h^\varepsilon$  decreases with decreasing  $\alpha$ . However, the basis functions of MsFEM-lin SUPG are independent of the multiplicative factor  $\alpha$ , which factors out in (16). Consequently, the oscillations of the basis functions of MsFEM-lin SUPG are too large when the advective term strongly dominates the diffusion. On the other hand, the  $\mathbb{P}_1$  SUPG method encodes no fine-scale oscillations, which becomes a better approximation of the actual behaviour of  $u_h^\varepsilon$  in the  $H^1$  norm when  $\alpha$  decreases. The only methods that capture the oscillations correctly throughout the entire regime of diffusion strengths are Adv-MsFEM-lin-B and PG Adv-MsFEM-lin- $\beta$ .

For the sake of completeness, we have also computed the relative error in the entire domain  $\Omega$  (the  $H^1$  error on  $\Omega$  is then normalized by the  $H^1(\Omega)$ -norm of the reference solution). The results are shown on the right plot of Figure 3. We observe that the error is in fact dominated by the error in the boundary layer. The methods Adv-MsFEM-lin-B and PG Adv-MsFEM-lin- $\beta$  yield the best accuracy, since the basis function  $\phi_i^{\varepsilon, \text{adv}}$  in the last element displays a boundary layer as well. We comment again on this topic in Section 5.1.4 for a two-dimensional test case.

As a final observation for this one-dimensional test case, we point out that the accuracy outside the boundary layer element of Adv-MsFEM-lin-B (and of PG Adv-MsFEM-lin- $\beta$ ), although excellent and the best of all here, deteriorates over almost three orders of magnitude when  $\alpha$  decreases in the range studied. Note that Adv-MsFEM-lin-B would be exact for all  $\alpha$  if  $f$  were piecewise constant; the results of Figure 3 show that a perturbation of the piecewise constant situation has a relatively small impact on the accuracy of Adv-MsFEM-lin-B in the diffusion-dominated regime, but a significantly larger impact in the advection-dominated regime. The large increase in the error if we deviate from the piecewise constant situation when the advection is dominant suggests (and this is indeed the case) that we cannot expect high accuracy in more challenging situations such as

the advection-dominated regime in two-dimensional problems.

In our next Section 3.2, we explain why the above findings do not all generalize to higher dimensions. We will consider numerical experiments in the two-dimensional setting with a more efficient MsFEM variant in Section 5.

### 3.2 On the generalization to higher dimensions

It was observed in numerical experiments in [49] that Adv-MsFEM-lin is not stable in dimension 2, unlike the one-dimensional setting seen above. This is consistent with our arguments of Section 2.3 making a link between Adv-MsFEM-lin and the RFB method, and the fact (recalled in Section 2.1.2) that, in dimensions higher than one, the RFB method does not include sufficient stabilization features. See also our Figure 7 below. Similarly, we have numerically observed Adv-MsFEM-lin-B to not be stable in dimension 2 (results not shown), in contrast to the one-dimensional setting seen above. We will therefore propose another variant of Adv-MsFEM for stability in higher dimensions in the next section (this variant coincides with Adv-MsFEM-lin-B in dimension one). But first, we provide some elements of explanation for the stability of Adv-MsFEM-lin and Adv-MsFEM-lin-B in the one dimensional setting and their instability in higher dimensions.

We first consider Adv-MsFEM-lin-B and postpone our comments on Adv-MsFEM-lin. Let us rewrite the multiscale approximation  $u_{H,B}^{\varepsilon,\text{adv}}$  as a sum of coarse scale and multiscale parts. Using the expression (23) for the multiscale basis functions  $\phi_i^{\varepsilon,\text{adv}}$ , we can write

$$u_{H,B}^{\varepsilon,\text{adv}} = u_H + \sum_{K \in \mathcal{T}_H} \sum_{\alpha=1}^d \partial_\alpha (u_H|_K) \chi_K^{\varepsilon,\text{adv},\alpha} + \sum_{K \in \mathcal{T}_H} \beta_K B_K^{\varepsilon,\text{adv}}, \quad (28)$$

for some  $u_H \in V_H$  and  $\beta_K \in \mathbb{R}$ . We recall that the bubble basis function  $B_K^{\varepsilon,\text{adv}}$  is defined by (25) and that the numerical corrector  $\chi_K^{\varepsilon,\text{adv},\alpha}$  is defined by (22).

Let us temporarily focus on the case of constant coefficients. We hence replace the oscillatory operator  $\mathcal{L}^\varepsilon$  by the operator  $-m \Delta + b \cdot \nabla$  with constant coefficients  $m$  and  $b$ , and also consider a piecewise constant right-hand side  $f$ . In this particular constant setting, and keeping the notation of the oscillatory setting, we have  $\chi_K^{\varepsilon,\text{adv},\alpha} = -b_\alpha B_K^{\varepsilon,\text{adv}}$  where  $b_\alpha$  is the  $\alpha$ -th component of  $b$  (see Lemma B.1 in Appendix B), and we note that  $B_K^{\varepsilon,\text{adv}}$  actually coincides with the bubble function  $b_K$  earlier defined in (12). Following a procedure known as *static condensation* (we refer to [18] for a similar analysis), we test the discrete variational problem (27) against  $B_K^{\varepsilon,\text{adv}}$  to determine  $\beta_K$ . Then we test (27) against an arbitrary  $v_H^{\varepsilon,\text{adv}} \in V_H^{\varepsilon,\text{adv}}$ , which we also expand according to (23), to eventually obtain an effective scheme for the function  $u_H \in V_H$  introduced in (28). The detailed computations in Appendix B show (see (64) with (57)) that the scheme for  $u_H$  is exactly the  $\mathbb{P}_1$  SUPG scheme with a stabilization parameter taking the value (13) (where we recall that  $b_K = B_K^{\varepsilon,\text{adv}}$ ), which has also been identified in the literature as the stabilization parameter related to the RFB method. As we recalled in Section 2.1.2, even though this value is the ideal value yielding nodal exactness of  $u_H$  in the one-dimensional setting, it is too small in higher dimensions to achieve full stabilization. Spurious oscillations remain in  $u_H$ .

Still in the constant setting, the same computations (see Remark B.4 of Appendix B) performed for Adv-MsFEM-lin (without bubbles) show that the effective scheme for  $u_H \in V_H$  has the same left-hand side as the effective scheme for Adv-MsFEM-lin-B. Since the potential instabilities of the scheme do not originate from the right-hand side, our conclusions on Adv-MsFEM-lin-B carry over to Adv-MsFEM-lin: stability is only achieved in dimension one.



For the higher-dimensional case, we define and investigate in the next sections yet another variant of Adv-MsFEM defined in terms of basis functions which satisfy *weak* boundary conditions on the element boundaries, in contrast to those of Adv-MsFEM-lin and Adv-MsFEM-lin-B that satisfy (strong) Dirichlet conditions. For example, the basis functions we are going to consider include bubble functions that vanish *in a weak sense* on the element boundaries, in contrast to those of Adv-MsFEM-lin-B that satisfy homogeneous Dirichlet conditions. One may hope that such basis functions can better resolve the multiscale phenomena of the solution and therefore provide better stability properties. This will indeed be the conclusion of our numerical experiments in Section 5.

## 4 A nonconforming MsFEM with *weak* bubbles

We consider in this section a variant of MsFEM *with Crouzeix-Raviart type boundary conditions*. The latter method was first introduced in [48] for pure diffusion problems (and then abbreviated as MsFEM-CR). The multiscale basis functions then reduce to the classical  $\mathbb{P}_1$  Crouzeix-Raviart element when applied to constant diffusion, hence the name of the method. MsFEM-CR was found to be particularly advantageous when enriched with bubble functions for the resolution of equations in perforated domains in [47]. Under the acronym Adv-MsFEM-CR, the method has then been adapted in the spirit of Adv-MsFEM-lin for the numerical approximation of advection-diffusion problems, first without any enrichment by bubble functions in [49], and next, in the specific context of perforated domains again, with such an enrichment in [50, 23]. To the best of our knowledge, the insights into the stabilizing properties of this method that we present in this article are new.

The Crouzeix-Raviart variants of the methods all rely on functions for which continuity across, or vanishing along, the mesh element interfaces are defined *weakly*, in contrast to continuity and vanishing, say, in Adv-MsFEM-lin, which are defined upon assigning a definite value. To be more precise, we briefly introduce now the space to which our new bubble functions, the so-called weak bubbles we are going to make use of, belong (we postpone their complete definition until Section 4.2). We define, for each  $K \in \mathcal{T}_H$ , the space

$$H_{0,w}^1(K) = \left\{ v \in H^1(K) \text{ s.t. } \int_e v = 0 \text{ for all } e \in \mathcal{E}_H(K) \right\},$$

where  $\mathcal{E}_H(K)$  denotes the set of faces (or edges in dimension 2) of the coarse mesh element  $K$ . We then define the space of *weak bubbles* as

$$\mathcal{B}_H^w = \bigoplus_{K \in \mathcal{T}_H} H_{0,w}^1(K).$$

In particular, a Crouzeix-Raviart type approximation is *nonconforming*. The functional setting of the previous sections above is thus extended to the broken  $H^1$  space with weak continuity conditions, that is,

$$H_{0,w}^{1,w}(\mathcal{T}_H) = \left\{ v \in L^2(\Omega) \text{ s.t. } v|_K \in H^1(K) \text{ for all } K \in \mathcal{T}_H \text{ and } \int_e \llbracket v \rrbracket = 0 \text{ for all } e \in \mathcal{E}_H \right\},$$

where  $\mathcal{E}_H$  is the set of all faces of the mesh  $\mathcal{T}_H$  and  $\llbracket v \rrbracket$  denotes the jump of  $v$  over such a face  $e$ , or the trace of  $v$  on  $e$  if  $e$  lies on  $\partial\Omega$ . Functions in  $H_{0,w}^{1,w}(\mathcal{T}_H)$  are thus continuous *in average* on the internal edges of the mesh (in the sense that the average of their jump vanishes) and they vanish *in average* on the boundary  $\partial\Omega$  (i.e. their average on each edge lying on  $\partial\Omega$  vanishes). Equipped with the broken  $H^1$  norm

$$\|v\|_{H^1(\mathcal{T}_H)} = \left( \sum_{K \in \mathcal{T}_H} \|v\|_{H^1(K)}^2 \right)^{1/2},$$

the space  $H_{0,w}^{1,w}(\mathcal{T}_H)$  is a Hilbert space.

#### 4.1 The multiscale basis functions

We have recalled in (19) that the multiscale basis function  $\phi_i^{\varepsilon,\text{adv}} \in H_0^1(\Omega)$  of Adv-MsFEM-lin are defined, for all  $1 \leq i \leq N$ , by

$$\forall K \in \mathcal{T}_H, \quad \begin{cases} \forall v \in H_0^1(K), & a_K^\varepsilon(\phi_i^{\varepsilon,\text{adv}}, v) = 0, \\ \phi_i^{\varepsilon,\text{adv}} = \phi_i^{\mathbb{P}^1} & \text{on } \partial K, \end{cases} \quad (29)$$

where  $a_K^\varepsilon$  is the restriction of the bilinear form  $a^\varepsilon$  to  $H^1(K) \times H^1(K)$ . The adaptation of this definition to the setting of weak boundary conditions is as follows: for each face  $e \in \mathcal{E}_H^{\text{in}}$ , where  $\mathcal{E}_H^{\text{in}}$  denotes the set of faces of the mesh that do not lie on  $\partial\Omega$ , we introduce the basis function  $\phi_e^{\varepsilon,\text{adv}} \in H_{0,w}^{1,w}(\mathcal{T}_H)$  by the local variational problem

$$\forall K \in \mathcal{T}_H, \quad \begin{cases} \text{for all } v \in H_{0,w}^1(K), & a_K^\varepsilon(\phi_e^{\varepsilon,\text{adv}}, v) = 0, \\ \text{for each } h \in \mathcal{E}_H(K), & \frac{1}{|h|} \int_h \phi_e^{\varepsilon,\text{adv}} = \delta_{e,h}, \end{cases} \quad (30)$$

where, we recall,  $\delta_{e,h}$  denotes the Kronecker symbol. We then define the Adv-MsFEM-CR space as  $W_H^{\varepsilon,\text{adv}} = \text{Span} \left\{ \phi_e^{\varepsilon,\text{adv}}, e \in \mathcal{E}_H^{\text{in}} \right\}$ . Note that we use a different notation for this space than for the Adv-MsFEM-lin space, denoted  $V_H^{\varepsilon,\text{adv}}$  (see (20)).

It is unclear to us how to establish well-posedness of the problems (30) because the bilinear form  $a_K^\varepsilon$  is not coercive on  $H_{0,w}^1(K)$  in general. To circumvent the problem of well-posedness, we *could* choose to work with a different bilinear form based on a skew-symmetric formulation of the advective term in (1), but we do not proceed in this direction and explain why this is the case in Remark 4.2 below. In practice, we consider a discrete approximation of (30) on a fine mesh (see Section 5 for details on our computational approach).

The global problem in Adv-MsFEM-CR is now defined as follows (just as for (30), establishing the well-posedness of (31) is actually an open question): find  $w_H^{\varepsilon,\text{adv}} \in W_H^{\varepsilon,\text{adv}}$  such that

$$\forall v_H^{\varepsilon,\text{adv}} \in W_H^{\varepsilon,\text{adv}}, \quad \sum_{K \in \mathcal{T}_H} a_K^\varepsilon(w_H^{\varepsilon,\text{adv}}, v_H^{\varepsilon,\text{adv}}) = F(v_H^{\varepsilon,\text{adv}}). \quad (31)$$

Let us stress that the approximation space  $W_H^{\varepsilon,\text{adv}}$  is not a subspace of  $H_0^1(\Omega)$  for a two-fold reason (the Adv-MsFEM-CR method (31) is thus a nonconforming approximation of (4)): (i) functions in  $W_H^{\varepsilon,\text{adv}}$  may jump across internal edges of the mesh, and (ii) functions in  $W_H^{\varepsilon,\text{adv}}$  do not satisfy the strong homogeneous Dirichlet boundary condition on  $\partial\Omega$ . On that second point, we deviate from the definition of the Crouzeix-Raviart MsFEM-type methods introduced in [48, 47], where the homogeneous Dirichlet boundary condition on  $\partial\Omega$  is satisfied in a strong sense. In contrast to [48, 47], the methods considered in [23, 56, 42] satisfy the same weak boundary conditions on  $\partial\Omega$  as here.

In the one dimensional setting, where interfaces are zero-dimensional, weak continuity agrees with strong continuity. In that setting, the Adv-MsFEM-lin and the Adv-MsFEM-CR basis functions therefore evidently coincide, and it follows from our study of Section 3 and Figure 1 that the Adv-MsFEM-CR basis functions are substantially deformed under the influence of the advection

field when it is dominant. It turns out that, even in the two-dimensional setting, Adv-MsFEM-CR also exhibits deformed basis functions (see Figure 5) and does not bring a substantial added value with respect to Adv-MsFEM-lin. Thus the idea to follow up on Section 3, and enrich the multiscale space  $W_H^{\varepsilon, \text{adv}}$  with additional, this time weak, bubble functions.

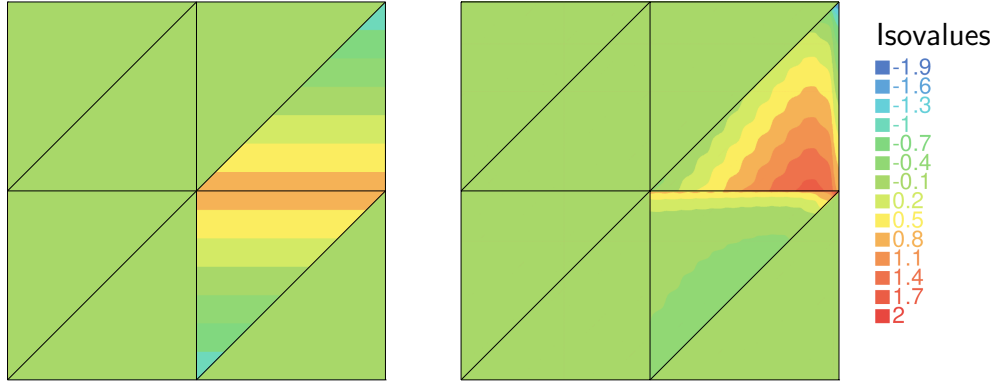


Figure 5: Comparison of the isovalues of a  $\mathbb{P}_1$  CR basis function (left) and an Adv-MsFEM-CR basis function (right) in the presence of a strong advection field. The advection field  $b$  is in the top right direction. The colour scale is identical on both figures.

## 4.2 Weak bubbles for Adv-MsFEM-CR

We now mimic the formulation (26), defining bubble functions  $B_K^{\varepsilon, \text{adv}} \in \mathcal{B}_H$ , in the case when bubble functions are *weak* and belong to the space  $\mathcal{B}_H^w$ . For each  $K \in \mathcal{T}_H$ , we define the weak bubble function  $B_K^{\varepsilon, \text{adv}, w}$  as the unique solution in  $H_{0,w}^1(K)$  to

$$\forall v \in H_{0,w}^1(K), \quad a_K^\varepsilon \left( B_K^{\varepsilon, \text{adv}, w}, v \right) = \int_K v. \quad (32)$$

The bubble function  $B_K^{\varepsilon, \text{adv}, w}$  in particular satisfies  $\mathcal{L}^\varepsilon B_K^{\varepsilon, \text{adv}, w} = 1$  in  $K$  and its average over each face of  $K$  vanishes. We extend  $B_K^{\varepsilon, \text{adv}, w}$  by 0 outside  $K$ . We next define the augmented multiscale space

$$W_{H,B}^{\varepsilon, \text{adv}} = W_H^{\varepsilon, \text{adv}} \bigoplus_{K \in \mathcal{T}_H} \text{Span} \left\{ B_K^{\varepsilon, \text{adv}, w} \right\},$$

and the variant of Adv-MsFEM-CR with weak bubbles, abbreviated as Adv-MsFEM-CR-B, as: find  $w_{H,B}^{\varepsilon, \text{adv}} \in W_{H,B}^{\varepsilon, \text{adv}}$  such that

$$\forall v_{H,B}^{\varepsilon, \text{adv}} \in W_{H,B}^{\varepsilon, \text{adv}}, \quad \sum_{K \in \mathcal{T}_H} a_K^\varepsilon \left( w_{H,B}^{\varepsilon, \text{adv}}, v_{H,B}^{\varepsilon, \text{adv}} \right) = F \left( v_{H,B}^{\varepsilon, \text{adv}} \right). \quad (33)$$

Similarly to (30) and (31), the well-posedness of (32) and (33) (and actually also of (34) below) remains an open question.

We are unfortunately unable to theoretically assess the quality of approximation of  $u^\varepsilon$  solution to (1) by  $w_{H,B}^{\varepsilon, \text{adv}}$  solution to (33). We have to rely on the numerical experiments of our Section 5, which show that  $w_{H,B}^{\varepsilon, \text{adv}}$  is indeed a stable and accurate approximation of  $u^\varepsilon$  in the advection-dominated regime. As for the theory, we are nevertheless able to show which function  $w_{H,B}^{\varepsilon, \text{adv}}$  naturally approximates at the infinite dimensional level. We indeed introduce, on the space  $H_{0,w}^{1,w}(\mathcal{T}_H)$ ,

the following problem: find  $\nu_H^\varepsilon \in H_{0,w}^{1,w}(\mathcal{T}_H)$  such that

$$\forall v \in H_{0,w}^{1,w}(\mathcal{T}_H), \quad \sum_{K \in \mathcal{T}_H} a_K^\varepsilon(\nu_H^\varepsilon, v) = F(v). \quad (34)$$

We note that, compared to the variational formulation (4) solved by  $u^\varepsilon$  solution to (1), the inter-element continuity (as well as the boundary condition on  $\partial\Omega$ ) is relaxed in (34). Jumps are allowed as long as the weak continuity condition of the space  $H_{0,w}^{1,w}(\mathcal{T}_H)$  is satisfied. To the best of our knowledge, this is an open question, and a nice track for further research regarding the theoretical stabilizing properties of Adv-MsFEM-CR, to know how close  $\nu_H^\varepsilon$ , solution to (34), and  $u^\varepsilon$ , solution to (4), are to one another.

We then have the following theoretical result (the proof of which is postponed until Appendix A), that somehow resembles Lemma 3.1 but holds true in any dimension, and not only in dimension one.

**Lemma 4.1.** *Suppose that  $f$  is piecewise constant on the coarse mesh and that the problems (30), (32), (33) and (34) all have a unique solution. Then Adv-MsFEM-CR-B provides the exact solution to (34), that is,  $w_{H,B}^{\varepsilon,\text{adv}} = \nu_H^\varepsilon$ .*

**Remark 4.2** (Alternative variational formulation). We noted above that the bilinear form  $a_K^\varepsilon$  is not coercive on the space  $H_{0,w}^1(K)$ , so it is unclear how to show well-posedness of the definitions (30) and (32) of the basis functions. A skew-symmetrized version of the advection term is frequently used in the literature, see e.g. [44, 50]. It is defined, for any  $u, v \in H^1(K)$ , as

$$a_K^{\varepsilon,\text{SS}}(u, v) = \int_K \nabla v \cdot A^\varepsilon \nabla u + \frac{1}{2} v b \cdot \nabla u - \frac{1}{2} u b \cdot \nabla v - \frac{1}{2} u v \operatorname{div} b,$$

where the last term vanishes under the assumption (3). It is readily seen that  $a_K^{\varepsilon,\text{SS}}$  is coercive on  $H_0^1(K)$ . Actually, the bilinear form  $a_K^{\varepsilon,\text{SS}}$  is also coercive on  $H_{0,w}^1(K)$  (see [48, Lemma 4.1]). For any  $u, v \in H_0^1(\Omega)$ , we evidently have  $\sum_{K \in \mathcal{T}_H} a_K^{\varepsilon,\text{SS}}(u, v) = a^\varepsilon(u, v)$ , by integration by parts. We

may thus replace  $a^\varepsilon$  by  $a^{\varepsilon,\text{SS}}$  throughout our developments without modifying the original solution of the problem (1). We have observed (numerical results not shown) that the variants of Adv-MsFEM using  $a_K^{\varepsilon,\text{SS}}$  are less accurate than those using  $a_K^\varepsilon$ . Why the results are of poor quality is unclear to us. From the theoretical standpoint, we however note that Lemma 4.1 remains true when  $a_K^\varepsilon$  is replaced by  $a_K^{\varepsilon,\text{SS}}$ , and the well-posedness of (30), (31), (32), (33) and (34) is guaranteed in this case.

**Remark 4.3.** Whether (33) can be used to stabilize (4) could in principle be studied in the constant coefficient case. Then (33) agrees with a  $\mathbb{P}_1$  Crouzeix-Raviart method with weak bubble functions. For Adv-MsFEM-lin and Adv-MsFEM-lin-B, the consideration of the classical RFB method for constant coefficients (and the reduction to an effective scheme in the *continuous*  $\mathbb{P}_1$  space  $V_H$ ) has allowed to better understand the multiscale setting itself, as seen above in Sections 2.3 and 3.2. We are not aware of similar studies for the (discontinuous)  $\mathbb{P}_1$  Crouzeix-Raviart FEM. For alternative stabilization approaches designed specifically for the  $\mathbb{P}_1$  Crouzeix-Raviart FEM, we refer to [44, 45, 24] and the bibliography therein.

### 4.3 A closer look at the (weak and strong) bubbles

We now investigate the role of the bubble functions in the linear systems resulting from the two Adv-MsFEM variants with bubbles, namely (27) (Adv-MsFEM-lin-B) and (33) (Adv-MsFEM-CR-B).

The notation of Adv-MsFEM-CR-B is employed throughout the section, but our analysis directly carries over to Adv-MsFEM-lin-B.

We denote by  $\left\{ \phi_e^{\varepsilon, \text{adv}} \right\}_{e \in \mathcal{E}_H^{\text{in}}}$  the basis for  $W_H^{\varepsilon, \text{adv}}$  and by  $\left\{ B_K^{\varepsilon, \text{adv}, w} \right\}_{K \in \mathcal{T}_H}$  that for the bubble space. The matrix of the linear system corresponding to (33) then is

$$\mathbb{A}^{\varepsilon, \text{adv}} = \left( \begin{array}{c|c} \mathbb{A}^{W,W} & \mathbb{A}^{W,B} \\ \hline \mathbb{A}^{B,W} & \mathbb{A}^{B,B} \end{array} \right), \quad (35)$$

where

$$\begin{aligned} \mathbb{A}_{h,e}^{W,W} &= \sum_{T \in \mathcal{T}_H} a_T^\varepsilon \left( \phi_e^{\varepsilon, \text{adv}}, \phi_h^{\varepsilon, \text{adv}} \right) \quad \text{for all } e, h \in \mathcal{E}_H^{\text{in}}, \\ \mathbb{A}_{K',K}^{B,B} &= \sum_{T \in \mathcal{T}_H} a_T^\varepsilon \left( B_K^{\varepsilon, \text{adv}, w}, B_{K'}^{\varepsilon, \text{adv}, w} \right) \quad \text{for all } K, K' \in \mathcal{T}_H, \\ \mathbb{A}_{h,K}^{W,B} &= \sum_{T \in \mathcal{T}_H} a_T^\varepsilon \left( B_K^{\varepsilon, \text{adv}, w}, \phi_h^{\varepsilon, \text{adv}} \right) \quad \text{for all } K \in \mathcal{T}_H, h \in \mathcal{E}_H^{\text{in}}, \\ \mathbb{A}_{K',e}^{B,W} &= \sum_{T \in \mathcal{T}_H} a_T^\varepsilon \left( \phi_e^{\varepsilon, \text{adv}}, B_{K'}^{\varepsilon, \text{adv}, w} \right) = 0 \quad \text{for all } e \in \mathcal{E}_H^{\text{in}}, K' \in \mathcal{T}_H. \end{aligned} \quad (36)$$

The lower left block  $\mathbb{A}^{B,W}$  vanishes because  $\phi_e^{\varepsilon, \text{adv}}$  solves (30) and  $B_{K'}^{\varepsilon, \text{adv}, w} \in H_{0,w}^1(K')$ . Moreover, the right lower block  $\mathbb{A}^{B,B}$  is diagonal because all bubble functions have disjoint support. Its diagonal entries are

$$\mathbb{A}_{K,K}^{B,B} = a_K^\varepsilon \left( B_K^{\varepsilon, \text{adv}, w}, B_K^{\varepsilon, \text{adv}, w} \right) = \int_K B_K^{\varepsilon, \text{adv}, w},$$

where we used (32). The bubble part  $w_B^{\varepsilon, \text{adv}} \in \text{Span} \left\{ B_K^{\varepsilon, \text{adv}, w}, K \in \mathcal{T}_H \right\}$  of the Adv-MsFEM-CR-B approximation  $w_{H,B}^{\varepsilon, \text{adv}} \in W_{H,B}^{\varepsilon, \text{adv}}$  is determined by the lower part of the linear system. Using the structure of the matrix  $\mathbb{A}^{\varepsilon, \text{adv}}$  revealed above, it can be explicitly computed, so that

$$w_B^{\varepsilon, \text{adv}} = \sum_{K \in \mathcal{T}_H} \frac{\int_K f B_K^{\varepsilon, \text{adv}, w}}{\int_K B_K^{\varepsilon, \text{adv}, w}} B_K^{\varepsilon, \text{adv}, w}. \quad (37)$$

If  $f$  is piecewise constant over the coarse mesh, this reduces to

$$w_B^{\varepsilon, \text{adv}} = \sum_{K \in \mathcal{T}_H} f|_K B_K^{\varepsilon, \text{adv}, w}. \quad (38)$$

With the explicit expression (37) for  $w_B^{\varepsilon, \text{adv}}$  at hand, we may now obtain a scheme for the remaining part  $w_W^{\varepsilon, \text{adv}} = w_{H,B}^{\varepsilon, \text{adv}} - w_B^{\varepsilon, \text{adv}} \in W_H^{\varepsilon, \text{adv}}$  of  $w_{H,B}^{\varepsilon, \text{adv}}$ . As pointed out above in Section 3.2, this is generally known as static condensation in the literature. The addition of bubble functions therefore does not increase the size of the linear system that has to be solved in order to compute  $w_{H,B}^{\varepsilon, \text{adv}}$  from (33) (with respect to the size of the linear system associated to (31) and corresponding to the Adv-MsFEM-CR method).

In the particular case when  $f$  is piecewise constant, upon inserting (38) in (33), the scheme

for  $w_W^{\varepsilon, \text{adv}}$  writes

$$\begin{aligned} \forall v_H^{\varepsilon, \text{adv}} \in W_H^{\varepsilon, \text{adv}}, \quad & \sum_{K \in \mathcal{T}_H} a_K^\varepsilon \left( w_W^{\varepsilon, \text{adv}}, v_H^{\varepsilon, \text{adv}} \right) \\ & = F \left( v_H^{\varepsilon, \text{adv}} \right) - \sum_{K \in \mathcal{T}_H} \left( \frac{1}{|K|} \int_K f \right) a_K^\varepsilon \left( B_K^{\varepsilon, \text{adv}, w}, v_H^{\varepsilon, \text{adv}} \right). \end{aligned} \quad (39a)$$

In fact, one can also compute  $w_W^{\varepsilon, \text{adv}}$  from (39a) when  $f$  is not piecewise constant. This results in a new numerical scheme that no longer coincides with Adv-MsFEM-CR-B for generic  $f$ . More precisely, we formulate the Adv-MsFEM-CR- $\beta$  variant as follows:

$$\text{Set } w_{H, \beta}^{\varepsilon, \text{adv}} = w_W^{\varepsilon, \text{adv}} + \sum_{K \in \mathcal{T}_H} \left( \frac{1}{|K|} \int_K f \right) B_K^{\varepsilon, \text{adv}, w}, \quad \text{where } w_W^{\varepsilon, \text{adv}} \text{ solves (39a).} \quad (39b)$$

An advantage of Adv-MsFEM-CR- $\beta$  is that, contrary to (37), the computation of the coefficients of the bubble functions does not require any integration at the microscale. The implications for the implementation of the Adv-MsFEM-CR- $\beta$  are further considered in Appendix C. The accuracy of Adv-MsFEM-CR-B and Adv-MsFEM-CR- $\beta$  are compared in Section 5.

#### 4.4 Petrov-Galerkin variants

In this section, we consider MsFEM methods in a Petrov-Galerkin formulation. This is indeed a standard idea to investigate when building multiscale approaches (see e.g. [29]) or when considering advection-diffusion problems (see e.g. [19, 53]). We also note that, as pointed out in [13, 12], Petrov-Galerkin variants of MsFEM are usually easier to implement (and actually amenable to a non-intrusive implementation) than Galerkin variants. We focus in this section on the Adv-MsFEM-CR variants, and we note that we could proceed similarly for the Adv-MsFEM-lin variants.

##### 4.4.1 The PG Adv-MsFEM-CR without bubbles

We first consider the following Petrov-Galerkin (PG) variant of the (Galerkin) Adv-MsFEM-CR method (31) (see Remark 4.4 below for another possibility): find  $w_H^{\varepsilon, \text{adv}, \text{PG}} \in W_H^{\varepsilon, \text{adv}}$  such that

$$\forall e \in \mathcal{E}_H^{\text{in}}, \quad \sum_{K \in \mathcal{T}_H} a_K^\varepsilon \left( w_H^{\varepsilon, \text{adv}, \text{PG}}, \phi_e^{\mathbb{P}_1} \right) = F \left( \phi_e^{\mathbb{P}_1} \right), \quad (40)$$

where the test functions  $\{\phi_e^{\mathbb{P}_1}\}_{e \in \mathcal{E}_H^{\text{in}}}$  are the standard  $\mathbb{P}_1$  Crouzeix-Raviart basis functions: the function  $\phi_e^{\mathbb{P}_1}$  belongs to  $H_{0,w}^{1,w}(\mathcal{T}_H)$ , is piecewise affine and is defined by the property  $\frac{1}{|h|} \int_h \phi_e^{\mathbb{P}_1} = \delta_{e,h}$  for each  $h \in \mathcal{E}_H$ . We denote  $V_H^w$  the  $\mathbb{P}_1$  Crouzeix-Raviart space:

$$V_H^w = \text{Span} \left\{ \phi_e^{\mathbb{P}_1}, e \in \mathcal{E}_H^{\text{in}} \right\}. \quad (41)$$

Note that, by construction, functions in  $V_H^w$  vanish (on average) on each edge of the mesh lying on  $\partial\Omega$ .

One may verify that the PG Adv-MsFEM-CR (40) and the Galerkin Adv-MsFEM-CR (31) lead to the same matrix in the linear system (see [12, Lemma 38]). In particular, any stabilizing properties of the multiscale approximation space that may be present in the Galerkin variant are preserved

within the Petrov-Galerkin variant. The variants (31) and (40) thus only differ in the right-hand side of the discrete formulation. For pure diffusion problems, the error analysis of [12] shows that the difference between the two variants converges to 0 at the rate  $O(H)$ , and the numerical examples (see [12, Figure 3]) show that, in practice, the two variants have the same accuracy (both in the case of Crouzeix-Raviart boundary conditions, as considered here, and of affine boundary conditions). For advection-diffusion problems, we numerically investigate this question in Section 5.1.5 below (see in particular Figure 12).

The MsFEM approach (40) falls in the general framework introduced in [12]. As shown there, it is thus amenable to a non-intrusive implementation (see Appendix C for details).

**Remark 4.4.** Another Petrov-Galerkin approach was proposed in [12, Sec. 5.3], which corresponds to taking, on the left-hand side of (40), multiscale test functions that locally solve the adjoint problem rather than the direct problem (we keep taking piecewise affine test functions on the right-hand side of (40)). It was shown in [12] that, for MsFEM methods without bubbles, this variant coincides with (40). This is however no longer the case when we add bubble functions to the approximation space. Since our numerical tests indicate that this approach is, when enriched with bubble functions, less accurate than both the Galerkin variant and the Petrov-Galerkin variant using piecewise affine test functions, we do not consider it further in this article.

#### 4.4.2 Extension to MsFEMs with bubbles

We now turn our attention to Adv-MsFEM-CR methods with bubbles, namely the Adv-MsFEM-CR- $\beta$  method (39b) and the Adv-MsFEM-CR-B method (33). We focus here on the former method, and can proceed similarly with the latter. The PG variant of Adv-MsFEM-CR- $\beta$  consists in setting

$$w_{H,\beta}^{\varepsilon,\text{adv},\text{PG}} = w_W^{\varepsilon,\text{adv},\text{PG}} + \sum_{K \in \mathcal{T}_H} \left( \frac{1}{|K|} \int_K f \right) B_K^{\varepsilon,\text{adv},w}, \quad (42a)$$

where  $w_W^{\varepsilon,\text{adv},\text{PG}} \in W_H^{\varepsilon,\text{adv}}$  solves

$$\forall v_H \in V_H^w, \quad \sum_{K \in \mathcal{T}_H} a_K^\varepsilon \left( w_W^{\varepsilon,\text{adv},\text{PG}}, v_H \right) = F(v_H) - \sum_{K \in \mathcal{T}_H} \left( \frac{1}{|K|} \int_K f \right) a_K^\varepsilon \left( B_K^{\varepsilon,\text{adv},w}, v_H \right), \quad (42b)$$

where we recall that  $V_H^w$  is the  $\mathbb{P}_1$  Crouzeix-Raviart space. The discrete problem (42b) is obtained from (39a) upon replacing all test functions by their piecewise affine Crouzeix-Raviart counterpart. The performances of (42) are numerically investigated in Section 5.1.5 below.

The MsFEM approach (42) does not fall in the general framework introduced in [12], because it includes bubble functions, a feature not considered there. A non-intrusive implementation of (42) is presented in Appendix C.

## 5 Numerical results

On two test cases for (1) set on the two-dimensional domain  $\Omega = (0, 1)^2$ , we present in this section a comparison of the various MsFEM and stabilization approaches discussed above. In both cases, the diffusion matrix is spherical and the right-hand side is given and slowly varying. The advection field is different from one case to the other, but, more importantly, the two cases essentially depart from one another in terms of the contrast imposed on the multiscale coefficient  $A^\varepsilon$ . When, as is the case in our second set of numerical tests, the contrast is larger, multiscale phenomena are expected to have a larger impact.

## 5.1 Moderate contrast (say of order 10)

Our first test case is

$$A^\varepsilon(x, y) = \mu^\varepsilon(x, y) \text{Id}, \quad \mu^\varepsilon(x, y) = \alpha \left( 1 + \frac{3}{4} \cos(2\pi x/\varepsilon) \sin(2\pi y/\varepsilon) \right), \quad (43a)$$

$$b(x, y) = \begin{pmatrix} 1 + y \\ 2 - x \end{pmatrix} / \sqrt{5 + 2y - 4x + y^2 + x^2}, \quad (43b)$$

$$f(x, y) = 2 + \sin(2\pi x) + x \cos(2\pi y), \quad (43c)$$

for different values of  $\alpha$  determining the relative importance of the advective and diffusive effects. The results are qualitatively the same for a similar test case with a constant advection field and constant right-hand side. Note that the advection field defined by (43b) is normalized (we have  $|b(x, y)| = 1$  everywhere on  $\Omega$ ) and divergence-free and thus satisfies the assumptions set in Section 2. This advection field, along with a reference solution, are shown on Figure 6. Given the orientation of the advection field, the boundary layer at the outflow can clearly be observed along the top and right sides of  $\Omega$ .

For MsFEM-lin SUPG (18), the stabilization parameter  $\tau$  is taken constant on each mesh element  $K \in \mathcal{T}_H$  with value

$$\tau = \frac{\text{diam}(K; b)}{2|b|} \left( \coth \text{Pe}_K - \frac{1}{\text{Pe}_K} \right) \quad \text{in } K, \quad (44)$$

as in [43], where  $\text{diam}(K; b)$  is the diameter of  $K$  in the direction of  $b$  and the element Péclet number  $\text{Pe}_K$  is defined as  $\text{Pe}_K = \frac{|b| \text{diam}(K; b)}{2\alpha}$ . In all these definitions, the advection field  $b$  (which is slowly varying) is evaluated at the centroid of  $K$ . In the one-dimensional case with piecewise constant coefficients, this choice of  $\tau$  corresponds to the optimal value providing a nodally exact solution, which was also characterized as (13) in the context of the RFB method. Note that, in the highly oscillatory case, it is not obvious to choose the value of the diffusion field to be used in the definition of  $\text{Pe}_K$ , because it may strongly vary within a single mesh element. Our choice here corresponds to the mean of the maximal and minimal values of  $\mu^\varepsilon$  in (43a) and is found to yield satisfactory results.

### 5.1.1 Stability

We first assess the stability of some MsFEM approaches on Figure 7. To this end, we define as follows the so-called  $\mathbb{P}_1$  part of the numerical solution: the numerical approximation is written as a sum of a piecewise affine function and numerical correctors, as in (23) for Adv-MsFEM-lin or (65) for Adv-MsFEM-CR, and the  $\mathbb{P}_1$  part of the MsFEM approximation is defined as the leftmost (piecewise affine) function on the right-hand side of (23) or (65) (the same decomposition can be made for methods including bubbles, see e.g. (28)). This piecewise affine component of the solution is sufficient to investigate stability. The numerical correctors (and the bubble basis functions, should they be used) indeed vanish (in a strong sense for the variants of MsFEM-lin, and on average for the variants of MsFEM-CR) on the edges of the coarse mesh elements, so they do not change the global behavior of the numerical approximation.

Figure 7 shows the  $\mathbb{P}_1$  part of the MsFEM approximation for some parameter values in the advection-dominated regime. Spurious oscillations that propagate far from the boundary layer are clearly visible, say along a vertical line at  $x = 0.5$ , for (unstabilized) MsFEM-lin and MsFEM-CR (this method, that we have not explicitly introduced in the article, consists in using basis functions



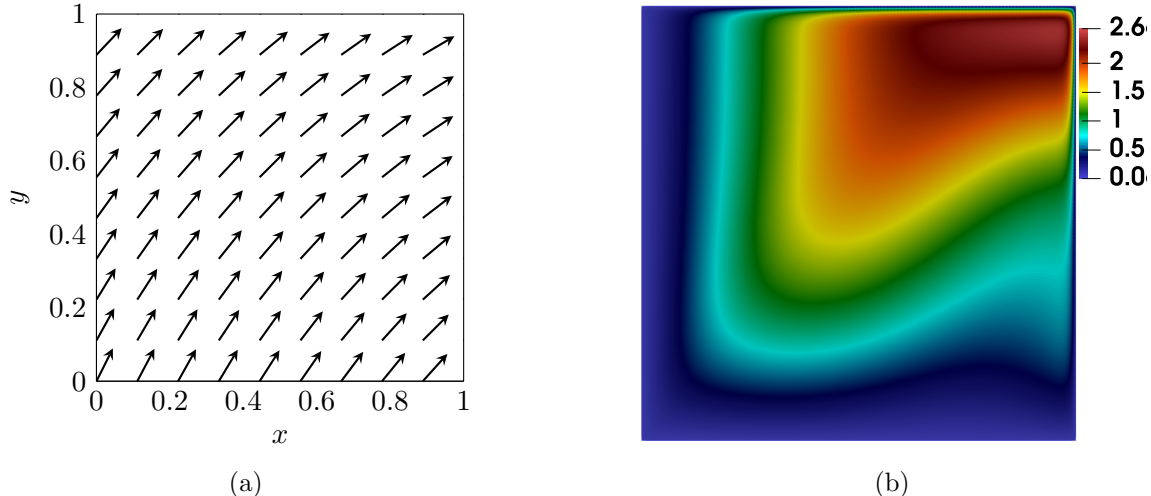


Figure 6: Test case (43). Left: Advection field (43b). Right: Example of a reference solution for  $\varepsilon = 2^{-7} \approx 8 \times 10^{-3}$  and  $\alpha = 2^{-7}$  (this solution has been computed by  $\mathbb{P}_1$  FEM with a meshsize  $h = 2^{-11}$ ).

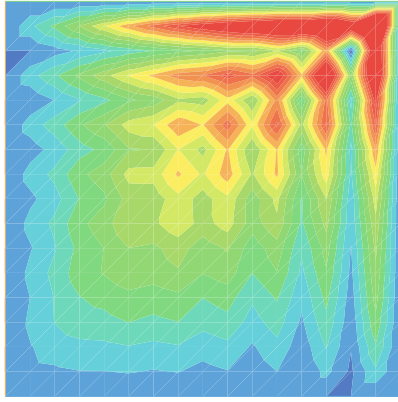
defined with only the diffusion part of the operator and satisfying Crouzeix-Raviart boundary conditions on the edges of the elements, and without any bubble function [48]; in the case of a constant diffusion coefficient, this method is simply the classical  $\mathbb{P}_1$  Crouzeix-Raviart FEM; we consider this method here for the sake of comparison with MsFEM-lin on the one hand and Adv-MsFEM-CR on the other hand). These spurious oscillations are removed from MsFEM-lin when we add the SUPG stabilization that was proposed in [49]. On the other hand, Adv-MsFEM-lin reduces the spurious oscillations but is not able to suppress them completely. The effective stabilization captured by the Adv-MsFEM-lin basis functions is too small, as is explained in Section 3.2. For Adv-MsFEM-CR, we see that no instabilities propagate outside the boundary layer. Better stabilizing effects are obtained from the numerical correctors in the space  $H_{0,w}^1(K)$  (satisfying weak boundary conditions) than from those in the traditional space  $H_0^1(K)$ .

Note that none of the MsFEM variants shown on Figure 7 use bubble functions. However, the  $\mathbb{P}_1$  part of the MsFEM variants including bubble functions turns out to actually be very close to that of the corresponding variant without bubbles. The equivalent of Figure 7 for MsFEM variants with bubbles is thus qualitatively identical to the current Figure 7. We recall that the bubble functions are introduced to maintain a good accuracy in the advection-dominated regime, when the multiscale basis functions associated to the nodes or to the edges are heavily deformed. We however observe that the stabilizing properties are already encoded in the numerical correctors. This observation generalizes the findings summarized in Remark 2.1 (which applies to bubbles with strong Dirichlet conditions) to the weak bubble framework.

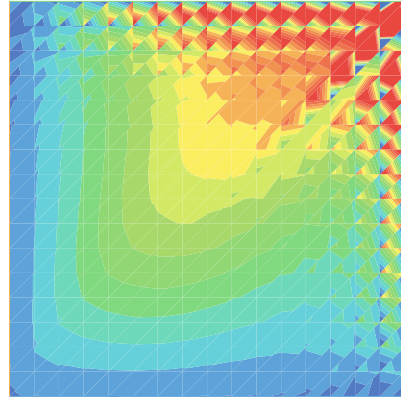
### 5.1.2 Measuring the error only outside the boundary layer

For the comparison of the approaches, we compute the error in  $H^1$ -norm. There is however a technicality, which we already briefly mentioned in the one-dimensional setting in Section 3.1, and upon which we briefly further comment here.

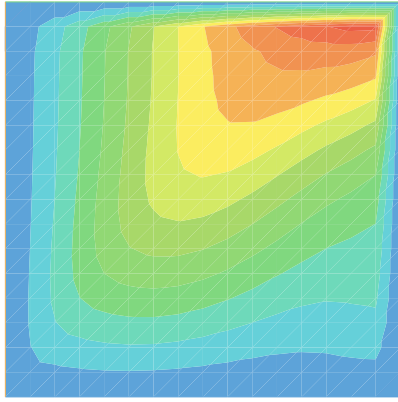
In the advection-dominated regime, the main challenging purpose of the numerical approximation is usually to correctly capture the solution (and foremost its large scale structure) *outside* the boundary layer. Within the boundary layer itself, standard finite elements can certainly not pretend



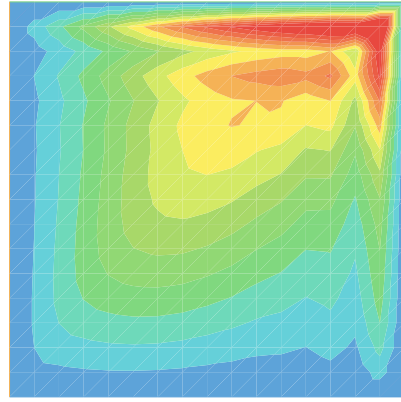
(a) MsFEM-lin (17)



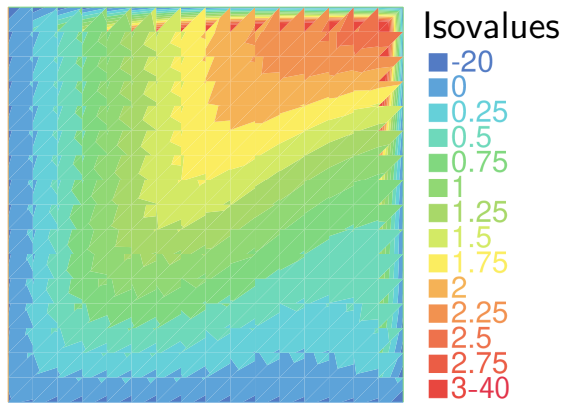
(b) MsFEM-CR



(c) MsFEM-lin SUPG (18)



(d) Adv-MsFEM-lin (21)



(e) Adv-MsFEM-CR (31)

Figure 7:  $\mathbb{P}_1$  part (as defined in the text) of various MsFEM approximations (all without bubbles) applied to the test case (43) when  $\varepsilon = 2^{-7}$ ,  $\alpha = 2^{-8}$ , and  $H = 2^{-4}$ . The colour code is the same for all figures (note that all the isovalues between 3 and 40, which correspond to overshoot regions, are represented by a single colour). The  $\mathbb{P}_1$  part of the (Adv)-MsFEM-CR variants belongs to the *discontinuous* Crouzeix-Raviart space (41), thus their sawtooth shape.

to recover the complex behavior of the solution, unless this boundary layer is itself meshed finely. The MsFEM variants (17) and (18) face the same difficulty. On the other hand, since the basis functions of the Adv-MsFEM variants we consider are adapted to the problem, there is some hope to adequately capture the profile of the solution within the boundary layer even using a coarse mesh. This is the reason why we successively consider the two issues.

We first measure the error of the numerical approximation outside all mesh elements  $K$  that contain a part of the boundary layer of  $u^\varepsilon$  that is visualized on Figure 6b (i.e. along the top and right sides of  $\Omega$ ). This region, called (as in Section 3.1) ‘outside the boundary layer mesh elements’ (OBLE), is again denoted by  $\Omega_{\text{OBLE}} = (0, 1 - H)^2$ , where  $H$  is the length of the legs of the mesh elements (see Figure 8). To be precise, we compute the errors in the following relative norm:

$$\|u_H - u_h^\varepsilon\|_{H^1(\mathcal{T}_H; \Omega_{\text{OBLE}}), \text{rel}} = \frac{\sqrt{\sum_{K \in \mathcal{T}_H, K \subset \Omega_{\text{OBLE}}} \|u_H - u_h^\varepsilon\|_{H^1(K)}^2}}{\|u_h^\varepsilon\|_{H^1(\Omega_{\text{OBLE}})}}, \quad (45)$$

for any numerical solution  $u_H$  that is piecewise  $H^1$ . Here,  $u_h^\varepsilon \in H^1(\Omega)$  is the  $\mathbb{P}_1$  approximation of (1) on a fine mesh (of mesh size  $h$  specified below).

Then, in a second stage (see Section 5.1.4 below), we will account for the boundary layer. The relative error will then be defined as

$$\|u_H - u_h^\varepsilon\|_{H^1(\mathcal{T}_H), \text{rel}} = \frac{\sqrt{\sum_{K \in \mathcal{T}_H} \|u_H - u_h^\varepsilon\|_{H^1(K)}^2}}{\|u_h^\varepsilon\|_{H^1(\Omega)}}. \quad (46)$$

instead of (45).

**Remark 5.1.** The normalization factor used in our definition (45) differs from that of our earlier work [49]. We use  $\|u_h^\varepsilon\|_{H^1(\Omega_{\text{OBLE}})}$ , whereas the earlier work used  $\|u_h^\varepsilon\|_{H^1(\Omega)}$ . Note that the latter norm (on the entire domain  $\Omega$ ) is unbounded in  $H^1(\Omega)$  as  $\alpha \rightarrow 0$ , because of the ever sharper boundary layer in  $\Omega \setminus \Omega_{\text{OBLE}}$ . This different choice does not qualitatively change the classification of the performance of the numerical methods at a fixed value of  $\alpha$ . The division by  $\|u_h^\varepsilon\|_{H^1(\Omega)}$  could give some biased impression that certain methods perform exceptionally well in the advection-dominated regime (for small  $\alpha$ ) because of a large normalization factor. Our choice of now normalizing by  $\|u_h^\varepsilon\|_{H^1(\Omega_{\text{OBLE}})}$  should better reflect the actual accuracy of the numerical methods.

As a matter of illustration, we recall with Figure 9 that evaluating the performance of numerical approaches on the basis of the error (45) indeed allows to discriminate between stable and unstable approaches. In that figure, we show the error (45) for a test case with constant coefficients, for the  $\mathbb{P}_1$  FEM and its stabilization by the SUPG method. When  $\alpha$  decreases, we observe that the error of the  $\mathbb{P}_1$  FEM grows by several orders of magnitude due to its instability. On the contrary, the error committed by the  $\mathbb{P}_1$  SUPG method outside the boundary layer is stable (and of the order of 10%) for all values of the diffusion coefficient. In contrast, if the error is defined by (46), then both methods are found to perform equally poorly, due to the inaccuracies in the boundary layer which dominate the error.

We next turn to a quantitative comparison of the MsFEM approaches, on the test case (43) with  $\varepsilon = 2^{-7}$ . On Figure 10, we compare the various numerical methods when using a coarse mesh with legs of size  $H = 2^{-4}$ , and for  $\alpha$  varying from  $2^{-1}$  to  $2^{-10} \approx 0.001$ . The fine mesh, used for the computation of the reference solution and the multiscale basis functions, has legs of length

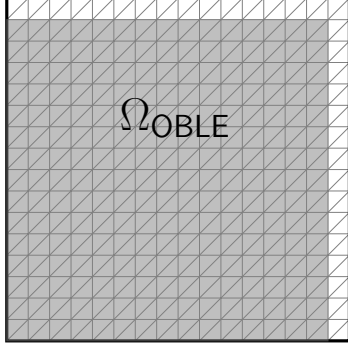


Figure 8: We measure the error outside the boundary layer elements, that is, in  $\Omega_{\text{OBLE}}$ , the domain highlighted in gray.

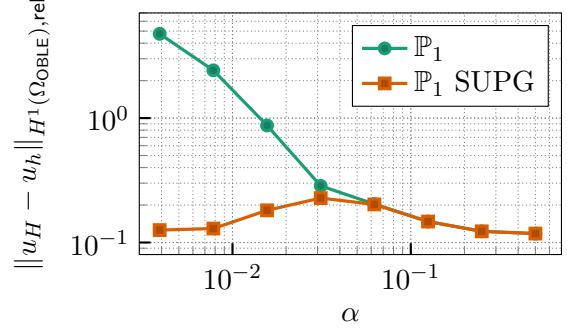


Figure 9: Relative errors (45) outside the boundary layer elements for  $\mathbb{P}_1$  FEMs for  $-\alpha \Delta u + b \cdot \nabla u = f$  on a coarse mesh  $\mathcal{T}_H$  with  $H = 2^{-4}$  ( $f = 1$  and  $b$  is a constant unit vector pointing in the top right direction).

$h = 2^{-11} = \varepsilon/16$  when  $\alpha \geq 2^{-9}$  and  $h = 2^{-12}$  when  $\alpha = 2^{-10}$ . The fine mesh is sufficiently fine to avoid instabilities of  $\mathbb{P}_1$  FEM, and to properly capture the oscillations of the diffusion coefficient. For the smallest value of  $\alpha$ , the fine mesh is refined because our original choice  $h = 2^{-11}$  did not allow to compute the Adv-MsFEM-CR basis functions correctly in our computations. All computations are executed with FREEFEM [33], and our code is available at [10].

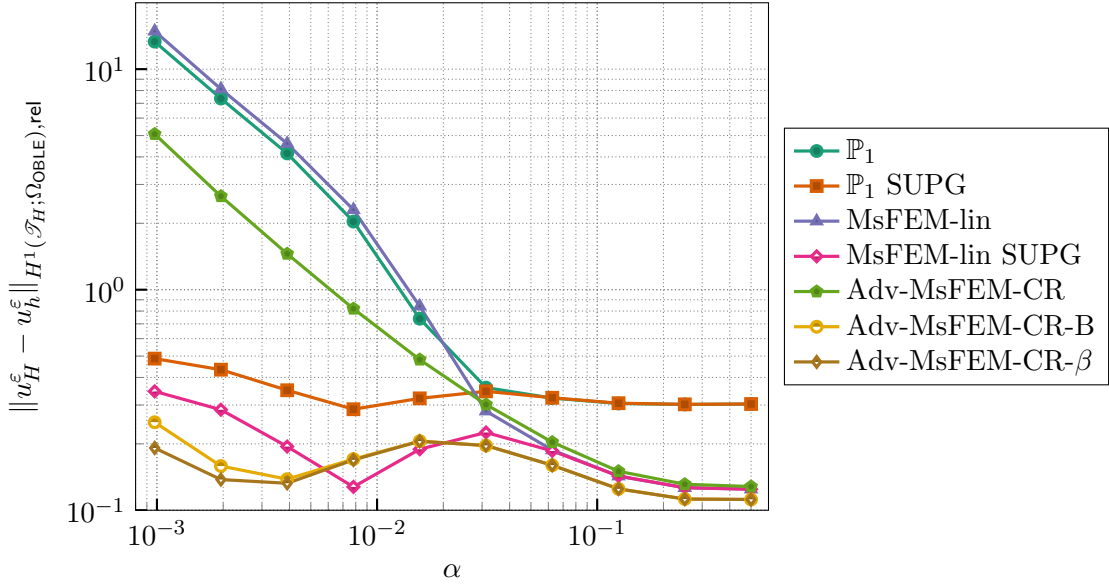


Figure 10: Relative errors (45) outside the boundary layer elements between the reference solution  $u_h^\varepsilon$  and various numerical approximations  $u_H^\varepsilon$ , for the test case (43) with  $\varepsilon = 2^{-7}$ ,  $H = 2^{-4}$  and various  $\alpha$ .

The instability of both  $\mathbb{P}_1$  FEM and MsFEM-lin is confirmed for small values of  $\alpha$  by the large relative errors observed even outside the boundary layer. In spite of the stability of Adv-MsFEM-CR that is observed on Figure 7, the accuracy of Adv-MsFEM-CR is also poor. This is not unexpected, given the strongly deformed multiscale functions in the space  $W_H^{\varepsilon, \text{adv}}$ . This phenomenon was also observed in the one-dimensional situation studied in Section 3.1. We further see that the accuracy

of MsFEM-lin SUPG and the two variants of Adv-MsFEM-CR with bubble functions is robust with respect to  $\alpha$ , showing the same fluctuations as the  $\mathbb{P}_1$  SUPG method in the single-scale case of Figure 9. We point out that Adv-MsFEM-CR-B and Adv-MsFEM-CR- $\beta$  are the only methods considered here, the accuracy of which does not depend on an adjusted additional stabilization parameter.

For the one-dimensional test case of Figure 3, it was observed in the advection-dominated regime that  $\mathbb{P}_1$  SUPG and Adv-MsFEM-lin-B have comparable accuracy and both outperform MsFEM-lin SUPG. Some elements of understanding were proposed with Figure 4, where we compared (as a function of the Péclet number) the amplitude of oscillations of the derivative of the reference solution with that of the numerical solutions. The same differences in the accuracy of the three methods cannot be observed for the two-dimensional tests on Figure 10. The  $\mathbb{P}_1$  SUPG method is now outperformed by MsFEM-lin SUPG and the two variants of Adv-MsFEM-CR with bubbles (Adv-MsFEM-CR-B and Adv-MsFEM-CR- $\beta$ ).

On the basis of these numerical results, we thus identify MsFEM-lin SUPG, Adv-MsFEM-CR-B and Adv-MsFEM-CR- $\beta$  as three approaches, the accuracy of which (outside the boundary layer) is robust with respect to the size of the advection. Discriminating among these approaches depends on the situation at hand. If the advection field is modified, then the basis functions of the latter two methods need to be recomputed. On the other hand, the latter two methods do not depend on the choice of a stabilization parameter, for which a correct value may be difficult to find when considering strongly heterogeneous media (this question is further discussed in Section 5.2 below). We also note that, for a given value of  $H$  (as is the case on Figure 10), the linear system to be solved in the online stage has the same dimension for the three methods (as a consequence of the static condensation argument alluded to above, including bubbles in the trial space does not increase the size of the global problem).

### 5.1.3 Delineating the advection-dominated regime

In simulations with slowly varying coefficients, the values of  $\alpha$ , and thus that of the local Péclet number, can be used as an indicator of the advection-dominated regime, that where  $\text{Pe}_K > 1$ . The same distinction is more delicate to make in the multiscale case, because it is unclear which specific value  $A^\varepsilon$  should be assigned for the definition of an ‘effective numerical Péclet number’. In the absence of a precise definition of the advection-dominated regime, the numerical comparison between  $\mathbb{P}_1$  and  $\mathbb{P}_1$  SUPG on the one hand, and between MsFEM-lin and MsFEM-lin SUPG on the other hand, provides an actual effective indicator. When the results provided by those approaches start to differ pairwise, the advection-dominated regime has presumably begun.

One may notice on Figure 10 that the accuracy of MsFEM-lin starts to degrade for larger values of  $\alpha$  than  $\mathbb{P}_1$  FEM (and this difference is even more noticeable on Figure 14 below). This can be explained as follows. We recall that, for a pure diffusion problem,  $\mathbb{P}_1$  FEM is equivalent to the  $\mathbb{P}_1$  approximation of an equation with a piecewise constant diffusion  $\bar{A}$  given by  $\bar{A}|_K = \frac{1}{|K|} \int_K A^\varepsilon$  for all  $K \in \mathcal{T}_H$ . For the advection-diffusion problem of interest here,  $\mathbb{P}_1$  FEM is equivalent to the  $\mathbb{P}_1$  approximation of an effective advection-diffusion equation with piecewise constant coefficients given, for all  $K \in \mathcal{T}_H$  and all  $1 \leq \alpha, \beta \leq d$ , by

$$\begin{aligned} \bar{A}_{\beta,\alpha}^{\mathbb{P}_1}|_K &= \frac{1}{|K|} a_K^\varepsilon (x^\alpha - x_{c,K}^\alpha, x^\beta - x_{c,K}^\beta) = \frac{1}{|K|} \int_K [A^\varepsilon]_{\beta,\alpha} + \frac{1}{|K|} \int_K b_\alpha (x^\beta - x_{c,K}^\beta), \\ \bar{b}_\alpha^{\mathbb{P}_1}|_K &= \frac{1}{|K|} a_K^\varepsilon (x^\alpha - x_{c,K}^\alpha, 1) = \frac{1}{|K|} \int_K b_\alpha, \end{aligned} \quad (47)$$

where we recall that  $x_{c,K} = (x_{c,K}^1, \dots, x_{c,K}^d)$  is the centroid of  $K$ . Since  $b$  is slowly-varying, we can neglect the second term in the right-hand side of (47) and approximate  $\overline{A}^{\mathbb{P}_1}|_K$  by the spherical matrix  $\frac{1}{|K|} \int_K A^\varepsilon$ . The start of the advection-dominated regime, in the sense that spurious oscillations appear in the numerical solution, depends on the local Péclet number  $(|\overline{b}^{\mathbb{P}_1}|_H) / (2\overline{A}^{\mathbb{P}_1})$  associated to the effective scheme.

Similarly, MsFEM-lin is equivalent to the  $\mathbb{P}_1$  approximation of an effective advection-diffusion equation with piecewise constant coefficients given, for all  $K \in \mathcal{T}_H$  and all  $1 \leq \alpha, \beta \leq d$ , by

$$\overline{A}_{\beta,\alpha}^{\text{MsFEM-lin}}|_K = \frac{1}{|K|} a_K^\varepsilon \left( x^\alpha - x_{c,K}^\alpha + \chi_K^{\varepsilon,\alpha}, x^\beta - x_{c,K}^\beta + \chi_K^{\varepsilon,\beta} \right), \quad (48)$$

$$\overline{b}_\alpha^{\text{MsFEM-lin}}|_K = \frac{1}{|K|} a_K^\varepsilon \left( x^\alpha - x_{c,K}^\alpha + \chi_K^{\varepsilon,\alpha}, 1 \right) = \frac{1}{|K|} \int_K b \cdot (e_\alpha + \nabla \chi_K^{\varepsilon,\alpha}) = \frac{1}{|K|} \int_K b_\alpha, \quad (49)$$

where  $\chi_K^{\varepsilon,\alpha} \in H_0^1(K)$  solves  $-\text{div}(A^\varepsilon \nabla (\chi_K^{\varepsilon,\alpha} + x^\alpha)) = 0$ , and where  $e_\alpha$  denotes the  $\alpha$ -th canonical unit vector of  $\mathbb{R}^d$ . The last equality in (49) stems from the fact that  $b$  is divergence-free. As for the  $\mathbb{P}_1$  method, the start of the advection-dominated regime depends on the local Péclet number associated to the effective scheme.

We observe that  $\overline{b}^{\mathbb{P}_1} = \overline{b}^{\text{MsFEM-lin}}$ . In addition, numerical computations show that, at a given value of  $\alpha$  in (43), the eigenvalues of the effective diffusion matrix  $\overline{A}^{\text{MsFEM-lin}}$  are smaller than those of  $\overline{A}^{\mathbb{P}_1}$  (in the particular case of a pure diffusion problem,  $\overline{A}^{\text{MsFEM-lin}}$  is actually an accurate approximation of the homogenized matrix, which is well-known to be smaller than the average of the oscillatory coefficient, which itself is equal to  $\overline{A}^{\mathbb{P}_1}$ ). The effective diffusion felt with the MsFEM-lin approach is thus smaller than that with the  $\mathbb{P}_1$  FEM. Spurious oscillations therefore appear sooner (i.e. for larger values of  $\alpha$ ) when one uses MsFEM-lin rather than  $\mathbb{P}_1$  FEM.

#### 5.1.4 Errors in the entire domain, including the boundary layer

In contrast to Section 5.1.2, we now consider on Figure 11 the relative errors on the *entire* domain  $\Omega$  of those numerical methods that were previously identified as stable. We measure these errors in the relative  $H^1$ -norm defined in (46). The denominator in the error (46) is much larger than in the error (45) that we used on Figure 10, precisely because of the large gradient of the reference solution within the boundary layer. The numerator in (46) is likewise by far dominated by the error in the boundary layer elements, i.e., in  $\Omega \setminus \Omega_{\text{OBL}}$ . The conclusions from Figure 11 are clear: the trial functions of the  $\mathbb{P}_1$  SUPG method and the MsFEM-lin SUPG are not adapted to the exponential decay of  $u_h^\varepsilon$  in the boundary layer and commit a large error in the advection-dominated regime. The only methods that are capable of resolving the boundary layer are the Adv-MsFEM-CR variants with or without bubbles. Note that this is achieved while no a priori information about the location of the boundary layer of the exact solution is encoded in the multiscale approximation space. The basis functions of Adv-MsFEM-lin (and Adv-MsFEM-lin-B) may provide an even better approximation of the boundary layer, because the boundary condition is enforced in a strong sense, like in the continuous problem (1). However, as a result of the incomplete stabilization of Adv-MsFEM-lin and Adv-MsFEM-lin-B, the resulting approximations do not capture the boundary layer of  $u^\varepsilon$  properly due to a large overshoot in this region.

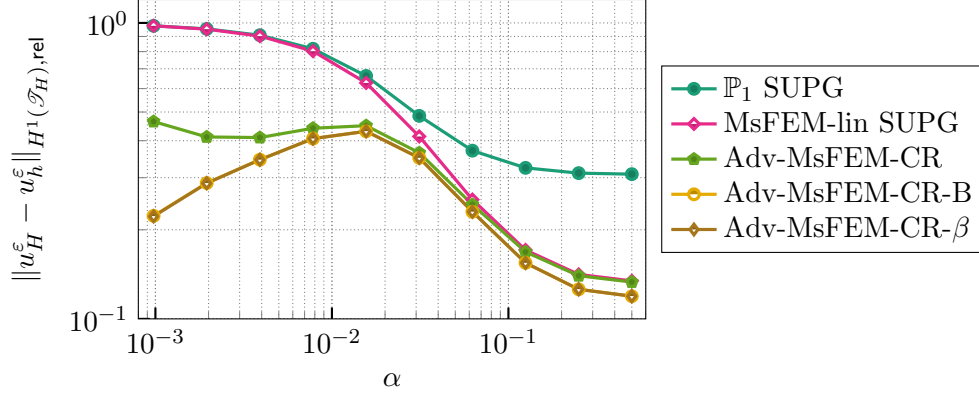


Figure 11: Relative errors (46) on the entire domain between the reference solution  $u_h^\varepsilon$  and various numerical approximations  $u_H^\varepsilon$ , for the test case (43) with  $\varepsilon = 2^{-7}$ ,  $H = 2^{-4}$  and various  $\alpha$ . At the scale of the figure, the results for Adv-MsFEM-CR-B and for Adv-MsFEM-CR- $\beta$  visually coincide.

### 5.1.5 Petrov-Galerkin variants

We now compare the MsFEM variants studied above (which are of Galerkin type) with the Petrov-Galerkin variants introduced in Section 4.4. On Figure 12, we compare the Galerkin variants of Adv-MsFEM-CR-B (defined by (33)) and Adv-MsFEM-CR- $\beta$  (defined by (39)) with the Petrov-Galerkin variants where, for each edge  $e \in \mathcal{E}_H^{in}$ , the multiscale test function  $\phi_e^{\varepsilon, \text{adv}}$  is replaced by the piecewise affine test function  $\phi_e^{\mathbb{P}_1} \in V_H^w$  (see (42) for the explicit formulation in the case of Adv-MsFEM-CR- $\beta$ ). Similarly, one can define a Petrov-Galerkin variant of MsFEM-lin SUPG (defined by (18)), the test space being  $V_H$  in this case.

As noted in Section 4.4.2, the above change of test functions does not affect the matrix of the linear system associated to either of the two Adv-MsFEM-CR methods with bubbles. The results of Figure 12 show that the accuracy of these two variants remains unaffected when changing to a Petrov-Galerkin method. On the other hand, this change of test functions affects the matrix of the linear system associated to MsFEM-lin SUPG, and we observe that its accuracy deteriorates in the advection-dominated regime when the test functions are changed to  $\mathbb{P}_1$  basis functions.

## 5.2 Larger contrast (say of order 100)

With a larger contrast within the diffusion coefficient, the difference between multiscale and standard FEM is expected to be more pronounced, at least in the diffusion-dominated regime. Investigating this regime is the purpose of the present section. We consider

$$A^\varepsilon(x, y) = \mu^\varepsilon(x, y) \text{Id}, \quad \mu^\varepsilon(x, y) = \alpha (1 + 100 \cos^2(\pi x/\varepsilon) \sin^2(\pi y/\varepsilon)), \quad (50a)$$

$$b(x, y) = \begin{pmatrix} 50 \cos(0.3\pi) \\ 50 \sin(0.3\pi) \end{pmatrix}, \quad (50b)$$

$$f(x, y) = 2 + \sin(2\pi x) + x \cos(2\pi y), \quad (50c)$$

where the right-hand side (50c) is equal to (43c), but the contrast in (50a) and the advection field (50b) have changed with respect to our previous test case. We now choose  $\varepsilon = \pi/150 \approx 0.02$ . The advection field is now uniform but not normalized, in contrast to (43b): its norm has been multiplied by 50. The mean of the maximal and minimal values values of  $\mu^\varepsilon$  in the diffusion coefficient has also changed, by a multiplicative factor of 50 in comparison to (43a). Like in Section 5.1,

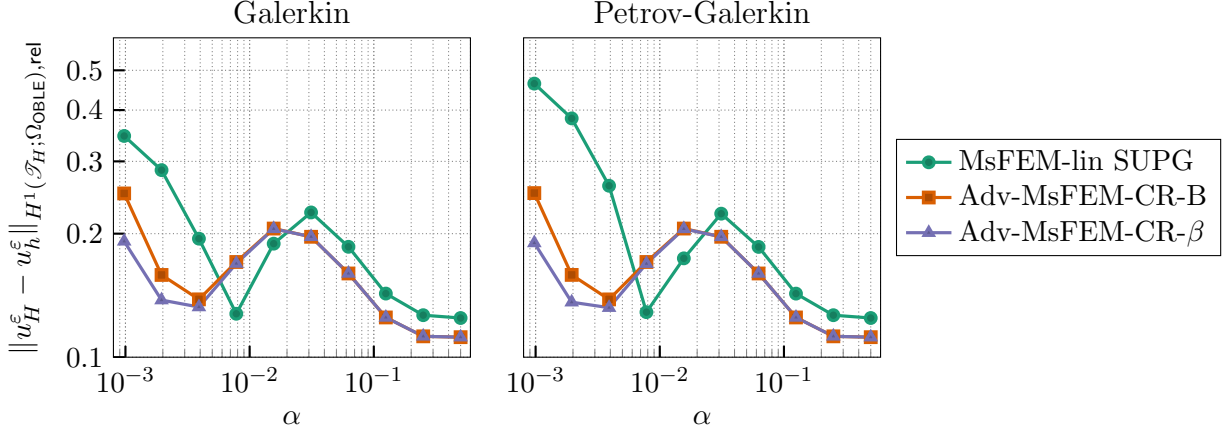


Figure 12: Comparison of some MsFEM variants in Galerkin and in Petrov-Galerkin formulation (with  $\mathbb{P}_1$  continuous test functions for MsFEM-lin SUPG, and  $\mathbb{P}_1$  Crouzeix-Raviart test functions for the two Adv-MsFEM-CR methods with bubbles). The test case is (43) with  $\varepsilon = 2^{-7}$ ,  $H = 2^{-4}$  and various  $\alpha$ , and we show the relative error (45).

the stabilization parameter  $\tau$  of MsFEM-lin SUPG is given by (44), where the element Péclet number  $\text{Pe}_K$  is again based on the mean of the minimal and maximal values of  $\mu^\varepsilon$ . For a given value of  $\alpha$  and  $H$ , the element Péclet number  $\text{Pe}_K$  has thus an identical value for the test cases considered here and in Section 5.1. The reference solution (for  $\varepsilon = \pi/150 \approx 0.02$  and  $\alpha = 2^{-5} \approx 0.03$ ) is shown on Figure 13 (it has been computed by  $\mathbb{P}_1$  FEM with a meshsize  $h = 2^{-11}$ ). Given the orientation of the advection field, the boundary layer at the outflow can clearly be observed along the top and right sides of  $\Omega$ .

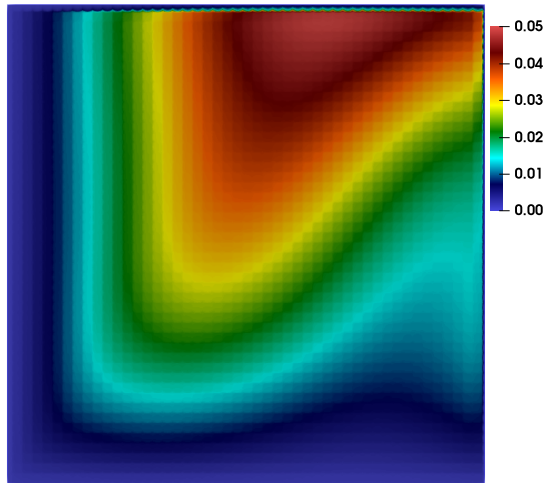


Figure 13: Reference solution for the test-case (50) with  $\varepsilon = \pi/150 \approx 0.02$  and  $\alpha = 2^{-5} \approx 0.03$ .

The error of the various numerical approaches for  $\alpha = 2^k$  for  $k = 2, \dots, -6$  (i.e. from  $\alpha = 4$  to  $\alpha \approx 1.5 \times 10^{-2}$ ) is shown on Figure 14, for two values of the coarse mesh size  $H$ . The fine mesh size is  $h = 2^{-11}$  except for the smallest value of  $\alpha$ , which again requires a fine mesh size of  $h = 2^{-12}$ .



We note that we have observed numerically that the accuracy of MsFEM-lin SUPG depends strongly on the precise value of the diffusion that is used in the definition of  $\text{Pe}_K$ . Especially in the high-contrast case, one risks taking a value that is either too small or too large, and even more so when  $\mu^\varepsilon$  has a more complicated, non-periodic structure. Too small a value for the diffusion results in too large a value for  $\text{Pe}_K$  and thus leads to an exceedingly diffusive scheme in the diffusion dominated regime. On the other hand, too large a value for the diffusion in the element Péclet number may decrease the stabilization of the method and deteriorate its accuracy in the advection-dominated regime. It is thus delicate to find a correct expression for the stabilization parameter  $\tau$  in strongly heterogeneous media, and we consider it useful to introduce alternative methods, namely Adv-MsFEM-CR-B and Adv-MsFEM-CR- $\beta$ , that are free from such a parameter and are yet robust with respect to the diffusion strength.

**Remark 5.2.** We mention in passing an alternative option to choose the stabilization parameter for MsFEM-lin SUPG that bypasses the ambiguity due to the heterogeneous character of  $\mu^\varepsilon$ . As explained in Section 5.1.3, we can recast MsFEM-lin as a  $\mathbb{P}_1$  FEM on an effective advection-diffusion equation, with piecewise constant coefficients given by (48)–(49). An option would thus consist in identifying a suitable stabilization parameter for that effective advection-diffusion equation (note that the fact that the effective diffusion matrix is non spherical may raise some difficulties), and using it in the MsFEM-lin SUPG scheme. We did not proceed in this direction.

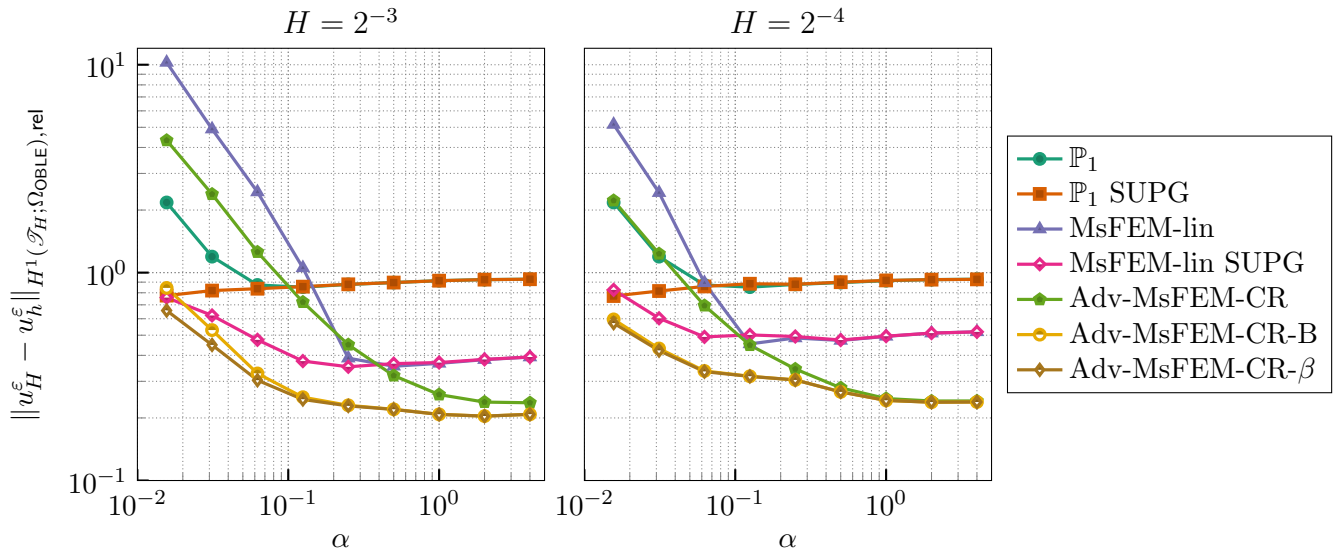


Figure 14: Relative errors (45) outside the boundary layer elements between the reference solution  $u_h^\varepsilon$  and various numerical approximations  $u_H^\varepsilon$ , for the test case (50) with  $\varepsilon \approx 0.02$ , two values of  $H$  and various  $\alpha$ .

On Figure 14, we see that the results for the two values of  $H$  are similar, although advection-dominating effects, for a given value of  $\alpha$ , are smaller when  $H$  is smaller. This is not unexpected, since the local Péclet number decreases when  $H$  decreases. We observe that the error of the multiscale methods increases slightly if  $H$  decreases from  $H = 2^{-3}$  to  $H = 2^{-4}$ . This presumably owes to the so-called resonance effect, that is routinely observed in the literature and slows down the convergence of MsFEMs when the discretization size  $H$  is close to the typical length scale of the microstructure.

As on Figure 10, but this is now more pronounced, one observes on Figure 14 that  $\mathbb{P}_1$  FEM, MsFEM-lin and Adv-MFEM-CR all perform poorly in the advection-dominated regime. On the other hand, MsFEM-lin SUPG, Adv-MsFEM-CR-B and Adv-MsFEM-CR- $\beta$  perform well in both the regimes where advection dominates and where diffusion dominates. We underline that the Adv-MsFEM-CR variants with additional bubble functions are the only such methods that do not depend on the choice of an additional (stabilization) parameter, for which a correct value is difficult to find when considering heterogeneous media.

## Appendices

### A Proof of Lemmas 2.3, 3.1 and 4.1

#### A.1 Proof of Lemma 2.3

Consider the one-dimensional variational formulation

$$\begin{cases} \forall v \in H_0^1(\Omega), & a^\varepsilon(u^\varepsilon, v) = 0, \\ u^\varepsilon(0) = u_0, & u^\varepsilon(1) = u_1, \end{cases} \quad (51)$$

of the equation in (1) with vanishing right-hand side and arbitrary boundary conditions  $u_0, u_1 \in \mathbb{R}$ . The interval  $\Omega = (0, 1)$  is divided into  $N + 1$  intervals  $(0, x_1) = (x_0, x_1), \dots, (x_N, x_{N+1}) = (x_N, 1)$ . For each  $i = 0, \dots, N + 1$ , a basis function for Adv-MsFEM-lin is defined by  $\mathcal{L}^\varepsilon \phi_i^{\varepsilon, \text{adv}} = 0$  inside each interval and  $\phi_i^{\varepsilon, \text{adv}}(x_j) = \delta_{i,j}$  for each  $j = 0, \dots, N + 1$ . It thus satisfies

$$\forall v \in H_0^1(x_j, x_{j+1}), \quad a^\varepsilon(\phi_i^{\varepsilon, \text{adv}}, v) = 0 \quad (52)$$

for all  $j = 0, \dots, N$ . The Adv-MsFEM-lin approximation of  $u^\varepsilon$  is then defined as the unique solution  $u_H^{\varepsilon, \text{adv}} \in V_H^{\varepsilon, \text{adv}} = \text{Span}\{\phi_i^{\varepsilon, \text{adv}}, 0 \leq i \leq N + 1\}$  to

$$\begin{cases} \forall v_H^{\varepsilon, \text{adv}} \in V_H^{\varepsilon, \text{adv}} \cap H_0^1(\Omega), & a^\varepsilon(u_H^{\varepsilon, \text{adv}}, v_H^{\varepsilon, \text{adv}}) = 0, \\ u_H^{\varepsilon, \text{adv}}(0) = u_0, & u_H^{\varepsilon, \text{adv}}(1) = u_1, \end{cases} \quad (53)$$

where we of course have  $V_H^{\varepsilon, \text{adv}} \cap H_0^1(\Omega) = \text{Span}\{\phi_i^{\varepsilon, \text{adv}}, 1 \leq i \leq N\}$ . Proving Lemma 2.3 amounts to showing that  $u_H^{\varepsilon, \text{adv}}$  solves (51), which admits  $u^\varepsilon$  as unique solution. Let  $v \in H_0^1(\Omega)$  be arbitrary as in (51) and consider the interpolant  $\tilde{v} = \sum_{i=0}^{N+1} v(x_i) \phi_i^{\varepsilon, \text{adv}} \in V_H^{\varepsilon, \text{adv}} \cap H_0^1(\Omega)$ . Note that, for all  $j = 0, \dots, N$ , we have  $v - \tilde{v} \in H_0^1(x_j, x_{j+1})$ . Therefore,  $a^\varepsilon(u_H^{\varepsilon, \text{adv}}, v) = a^\varepsilon(u_H^{\varepsilon, \text{adv}}, v - \tilde{v}) + a^\varepsilon(u_H^{\varepsilon, \text{adv}}, \tilde{v}) = 0$ , since the first term and the second term both vanish, respectively because of (52) and (53). This concludes the proof.

#### A.2 Proof of Lemma 3.1

Let  $u^\varepsilon$  be the solution to (1). Define  $\tilde{u}_{H,B}^{\varepsilon, \text{adv}} \in V_{H,B}^{\varepsilon, \text{adv}}$  as

$$\tilde{u}_{H,B}^{\varepsilon, \text{adv}} = \sum_{i=1}^N u^\varepsilon(x_i) \phi_i^{\varepsilon, \text{adv}} + \sum_{K \in \mathcal{T}_H} f|_K B_K^{\varepsilon, \text{adv}},$$

where we recall that  $x_1, \dots, x_N$  are the internal nodes of the mesh. Since  $\tilde{u}_{H,B}^{\varepsilon,\text{adv}}$  and  $u^\varepsilon$  coincide on all nodes of the mesh, and since, by (19) and (25), it holds  $\mathcal{L}^\varepsilon \tilde{u}_{H,B}^{\varepsilon,\text{adv}} = f|_K = \mathcal{L}^\varepsilon u^\varepsilon$  in  $K$  for all  $K \in \mathcal{T}_H$ , it follows that  $\tilde{u}_{H,B}^{\varepsilon,\text{adv}} = u^\varepsilon$ . This shows that  $u^\varepsilon$  belongs to the approximation space  $V_{H,B}^{\varepsilon,\text{adv}}$ . Adv-MsFEM-lin-B is therefore exact by the classical Céa Lemma. This concludes the proof.

### A.3 Proof of Lemma 4.1

We show that  $\nu_H^\varepsilon$  belongs to the finite-dimensional space  $W_{H,B}^{\varepsilon,\text{adv}}$ . The function  $\varphi = \nu_H^\varepsilon - \sum_{K \in \mathcal{T}_H} f|_K B_K^{\varepsilon,\text{adv},w}$  satisfies, for any  $K \in \mathcal{T}_H$  and for any  $w \in H_{0,w}^1(K)$ ,

$$a_K^\varepsilon(\varphi, w) = a_K^\varepsilon(\nu_H^\varepsilon, w) - f|_K a_K^\varepsilon(B_K^{\varepsilon,\text{adv},w}, w) = \int_K f w - f|_K \int_K w = 0,$$

using (32) and (34) in the second equality and the fact that  $f$  is piecewise constant in the third equality. The function  $\varphi$  thus belongs to  $W_H^{\varepsilon,\text{adv}}$  (see (30)), which implies that  $\nu_H^\varepsilon \in W_{H,B}^{\varepsilon,\text{adv}}$ . We conclude the proof using the well-posedness of (33).

## B Derivation of the effective scheme for Adv-MsFEM-lin and Adv-MsFEM-lin-B in the case of constant coefficient problems

Writing the Adv-MsFEM-lin-B solution  $u_{H,B}^{\varepsilon,\text{adv}}$  as in (28), we derive here the effective scheme on the space  $V_H$  that defines  $u_H$  in the case of constant diffusion coefficient  $m$  and advection field  $b$  and piecewise constant right-hand side  $f$ . In passing, we also derive the effective scheme corresponding to Adv-MsFEM-lin (see Remark B.4). Although we keep, in this appendix, the notations from the oscillatory case, we underline that the differential operator  $\mathcal{L}^\varepsilon$  takes the form  $\mathcal{L}^\varepsilon u = -m \Delta u + b \cdot \nabla u$ . We start with some observations that can easily be verified by elementary computations and which will frequently be used in the computations that follow.

**Lemma B.1.** *Under the above assumptions of constant diffusion and advection fields, for each  $K \in \mathcal{T}_H$  and each  $1 \leq \alpha \leq d$ , the numerical corrector  $\chi_K^{\varepsilon,\text{adv},\alpha} \in H_0^1(K)$  defined by (22) satisfies  $\chi_K^{\varepsilon,\text{adv},\alpha} = -b_\alpha B_K^{\varepsilon,\text{adv}}$ , where  $B_K^{\varepsilon,\text{adv}}$  is defined by (25).*

**Lemma B.2.** *Let  $w_H^{\varepsilon,\text{adv}}$  be any function in the space  $V_H^{\varepsilon,\text{adv}}$  defined by (20) and let  $v, \bar{v}$  be any functions in  $H_0^1(\Omega)$  that share the same trace on the mesh interfaces. Then it follows from (19) that  $a^\varepsilon(w_H^{\varepsilon,\text{adv}}, \bar{v}) = a^\varepsilon(w_H^{\varepsilon,\text{adv}}, v)$ .*

**Lemma B.3.** *For any mesh element  $K \in \mathcal{T}_H$ , an integration by parts shows that the bubble function  $B_K^{\varepsilon,\text{adv}}$  defined by (25) satisfies  $\int_K \partial_\alpha B_K^{\varepsilon,\text{adv}} = 0$  for all  $\alpha = 1, \dots, d$ .*

Following a static condensation procedure, we first determine the coefficients  $\beta_K$  in (28). Let us denote the bubble part of  $u_{H,B}^{\varepsilon,\text{adv}}$  by  $u_B^{\varepsilon,\text{adv}} \in \bigoplus_{K \in \mathcal{T}_H} \text{Span}\{B_K^{\varepsilon,\text{adv}}\}$  and the remaining part of  $u_{H,B}^{\varepsilon,\text{adv}}$  by  $u_V^{\varepsilon,\text{adv}} \in V_H^{\varepsilon,\text{adv}}$ .

Fix a mesh element  $K \in \mathcal{T}_H$ . Testing (27) against  $B_K^{\varepsilon,\text{adv}}$ , and since  $u_{H,B}^{\varepsilon,\text{adv}} = u_V^{\varepsilon,\text{adv}} + u_B^{\varepsilon,\text{adv}}$ , we have

$$a^\varepsilon(u_V^{\varepsilon,\text{adv}}, B_K^{\varepsilon,\text{adv}}) + a^\varepsilon(u_B^{\varepsilon,\text{adv}}, B_K^{\varepsilon,\text{adv}}) = F(B_K^{\varepsilon,\text{adv}}) = \int_K f B_K^{\varepsilon,\text{adv}}.$$

Since  $B_K^{\varepsilon, \text{adv}} \in H_0^1(K)$ , the first term on the left-hand side vanishes by (29). Using that all bubble functions have disjoint supports, we obtain

$$\beta_K a_K^\varepsilon \left( B_K^{\varepsilon, \text{adv}}, B_K^{\varepsilon, \text{adv}} \right) = \int_K f B_K^{\varepsilon, \text{adv}}.$$

Next using (32) with  $B_K^{\varepsilon, \text{adv}}$  as test function, this simplifies to

$$\beta_K = f_K,$$

denoting by  $f_K$  the (constant) value of  $f$  on  $K$ . With this, the scheme (27) becomes

$$\forall v_{H,B}^{\varepsilon, \text{adv}} \in V_{H,B}^{\varepsilon, \text{adv}}, \quad a^\varepsilon \left( u_V^{\varepsilon, \text{adv}}, v_{H,B}^{\varepsilon, \text{adv}} \right) = \int_\Omega f v_{H,B}^{\varepsilon, \text{adv}} - \sum_{K \in \mathcal{T}_H} f_K a^\varepsilon \left( B_K^{\varepsilon, \text{adv}}, v_{H,B}^{\varepsilon, \text{adv}} \right).$$

Since this equation is satisfied for any test function equal to a bubble function  $B_K^{\varepsilon, \text{adv}}$ , it now suffices to restrict the test functions to the space  $V_H^{\varepsilon, \text{adv}}$  to determine  $u_V^{\varepsilon, \text{adv}}$ . For all computations below, we thus fix an arbitrary test function  $v_H^{\varepsilon, \text{adv}} \in V_H^{\varepsilon, \text{adv}}$ , for which we have

$$a^\varepsilon \left( u_V^{\varepsilon, \text{adv}}, v_H^{\varepsilon, \text{adv}} \right) = \int_\Omega f v_H^{\varepsilon, \text{adv}} - \sum_{K \in \mathcal{T}_H} f_K a^\varepsilon \left( B_K^{\varepsilon, \text{adv}}, v_H^{\varepsilon, \text{adv}} \right). \quad (54)$$

Let us first consider the left-hand side of (54). Expanding the multiscale basis function  $v_H^{\varepsilon, \text{adv}}$  according to (23), we obtain a (piecewise affine) function  $v_H \in V_H$  that is equal to  $v_H^{\varepsilon, \text{adv}}$  on all interfaces of the mesh. By Lemma B.2, we have

$$a^\varepsilon \left( u_V^{\varepsilon, \text{adv}}, v_H^{\varepsilon, \text{adv}} \right) = a^\varepsilon \left( u_V^{\varepsilon, \text{adv}}, v_H \right) = \sum_{K \in \mathcal{T}_H} \int_K m \nabla u_H^{\varepsilon, \text{adv}} \cdot \nabla v_H + v_H b \cdot \nabla u_H^{\varepsilon, \text{adv}}.$$

Expanding  $u_V^{\varepsilon, \text{adv}}$  itself in the spirit of (23) and using Lemma B.1, this can again be rewritten as

$$\begin{aligned} a^\varepsilon \left( u_V^{\varepsilon, \text{adv}}, v_H^{\varepsilon, \text{adv}} \right) &= \sum_{K \in \mathcal{T}_H} \int_K m \nabla u_H \cdot \nabla v_H + v_H b \cdot \nabla u_H \\ &\quad - \sum_{K \in \mathcal{T}_H} \sum_{\alpha=1}^d \int_K m \partial_\alpha u_H b_\alpha \nabla B_K^{\varepsilon, \text{adv}} \cdot \nabla v_H + v_H \partial_\alpha u_H b_\alpha b \cdot \nabla B_K^{\varepsilon, \text{adv}}, \end{aligned} \quad (55)$$

for some  $u_H \in V_H$ . Note that, for all  $\alpha = 1, \dots, d$ ,  $\partial_\alpha u_H$  is piecewise constant and  $b_\alpha$  is supposed constant throughout  $\Omega$ . Lemma B.3 thus shows that the first term on the second line of (55) vanishes. Performing an integration by parts on the second term and using that the bubble function  $B_K^{\varepsilon, \text{adv}}$  vanishes on element boundaries, we obtain that, for all  $K \in \mathcal{T}_H$ ,

$$- \sum_{\alpha=1}^d \int_K v_H \partial_\alpha u_H b_\alpha b \cdot \nabla B_K^{\varepsilon, \text{adv}} = \int_K (b \cdot \nabla u_H) (b \cdot \nabla v_H) B_K^{\varepsilon, \text{adv}}. \quad (56)$$

Note that  $b$ ,  $\nabla v_H$  and  $\nabla u_H$  are both constant inside each mesh element. Thus, upon defining, for all  $K \in \mathcal{T}_H$ , the piecewise constant stabilization parameter

$$\tau^B|_K = \frac{1}{|K|} \int_K B_K^{\varepsilon, \text{adv}}, \quad (57)$$

we obtain

$$\int_K (b \cdot \nabla u_H) (b \cdot \nabla v_H) B_K^{\varepsilon, \text{adv}} = \int_K \tau^B (b \cdot \nabla u_H) (b \cdot \nabla v_H). \quad (58)$$

Combining (55), (56) and (58), it follows that the left-hand side of (54) reads

$$a^\varepsilon \left( u_V^{\varepsilon, \text{adv}}, v_H^{\varepsilon, \text{adv}} \right) = \sum_{K \in \mathcal{T}_H} \int_K m \nabla u_H \cdot \nabla v_H + v_H b \cdot \nabla u_H + \tau^B (b \cdot \nabla u_H) (b \cdot \nabla v_H). \quad (59)$$

This is exactly the left-hand side of the  $\mathbb{P}_1$  SUPG scheme (6) with stabilization parameter  $\tau^B$ .

Regarding the first term of the right-hand side of (54), we obtain, using the same expansions as above,

$$\int_\Omega f v_H^{\varepsilon, \text{adv}} = \int_\Omega f v_H - \sum_{K \in \mathcal{T}_H} \sum_{\alpha=1}^d \int_K f \partial_\alpha v_H b_\alpha B_K^{\varepsilon, \text{adv}}.$$

Since  $f$ ,  $\partial_\alpha v_H$  and  $b_\alpha$  are constant in each mesh element  $K$ , we can again use the definition of the stabilization parameter  $\tau^B$  to find

$$\int_\Omega f v_H^{\varepsilon, \text{adv}} = \int_\Omega f v_H - \tau^B f b \cdot \nabla v_H. \quad (60)$$

**Remark B.4.** Consider momentarily the Adv-MsFEM-lin scheme (21) (without bubbles) instead of the Adv-MsFEM-lin-B scheme (27) as we have done so far in this Appendix. The problem then consists in finding  $u_H^{\varepsilon, \text{adv}} \in V_H^{\varepsilon, \text{adv}}$  such that  $a^\varepsilon \left( u_H^{\varepsilon, \text{adv}}, v_H^{\varepsilon, \text{adv}} \right) = F \left( v_H^{\varepsilon, \text{adv}} \right)$  for any  $v_H^{\varepsilon, \text{adv}} \in V_H^{\varepsilon, \text{adv}}$ . The identities (59) and (60) allow to recast the problem as: find  $u_H \in V_H$  such that

$$\begin{aligned} \forall v_H \in V_H, \quad \sum_{K \in \mathcal{T}_H} \int_K m \nabla u_H \cdot \nabla v_H + v_H b \cdot \nabla u_H + \tau^B (b \cdot \nabla u_H) (b \cdot \nabla v_H) \\ = \int_\Omega f v_H - \tau^B f b \cdot \nabla v_H, \end{aligned} \quad (61)$$

that we can also write in the form

$$\forall v_H \in V_H, \quad a^\varepsilon(u_H, v_H) + a_{\text{stab}}(u_H, v_H) = F(v_H) - F_{\text{stab}}(v_H),$$

where  $a_{\text{stab}}$  and  $F_{\text{stab}}$  are the stabilization terms defined by (10) and (8) with the stabilization parameter  $\tau^B$ . We thus see that Adv-MsFEM-lin applied to a constant coefficient problem corresponds to an effective  $\mathbb{P}_1$  scheme, the left-hand side of which coincides with the SUPG scheme with stabilization parameter  $\tau^B$ , but the right-hand side of which takes a negative sign in front of the stabilization term instead of a positive sign as in (6).

We eventually derive the contribution to the effective scheme of the second term in the right-hand side of (54). Fix a mesh element  $K$ . Again using (23) for  $v_H^{\varepsilon, \text{adv}}$  and Lemma B.1 for the numerical correctors in (23), we can write

$$a^\varepsilon \left( B_K^{\varepsilon, \text{adv}}, v_H^{\varepsilon, \text{adv}} \right) = a_K^\varepsilon \left( B_K^{\varepsilon, \text{adv}}, v_H^{\varepsilon, \text{adv}} \right) = a_K^\varepsilon \left( B_K^{\varepsilon, \text{adv}}, v_H \right) - \sum_{\alpha=1}^d a_K^\varepsilon \left( B_K^{\varepsilon, \text{adv}}, b_\alpha \partial_\alpha (v_H|_K) B_K^{\varepsilon, \text{adv}} \right). \quad (62)$$

For the first term on the right-hand side of (62), we have

$$a_K^\varepsilon \left( B_K^{\varepsilon, \text{adv}}, v_H \right) = \int_K m \nabla B_K^{\varepsilon, \text{adv}} \cdot \nabla v_H + v_H b \cdot \nabla B_K^{\varepsilon, \text{adv}}.$$

By Lemma B.3, the integral of the first term vanishes. An integration by parts for the second term leads to

$$a_K^\varepsilon \left( B_K^{\varepsilon, \text{adv}}, v_H \right) = - \int_K B_K^{\varepsilon, \text{adv}} b \cdot \nabla v_H = - \int_K \tau^B b \cdot \nabla v_H,$$

the second equality being true because  $\nabla v_H$  and  $b$  are constant in  $K$ .

We rewrite the second term on the right-hand side of (62) using (26), which implies

$$\sum_{\alpha=1}^d a_K^\varepsilon \left( B_K^{\varepsilon, \text{adv}}, b_\alpha \partial_\alpha (v_H|_K) B_K^{\varepsilon, \text{adv}} \right) = \int_K B_K^{\varepsilon, \text{adv}} b \cdot \nabla v_H = \int_K \tau^B b \cdot \nabla v_H.$$

The second term in the right-hand side of (54) thus reads

$$\sum_{K \in \mathcal{T}_H} f_K a_K^\varepsilon \left( B_K^{\varepsilon, \text{adv}}, v_H^{\varepsilon, \text{adv}} \right) = -2 \int_\Omega \tau^B f b \cdot \nabla v_H, \quad (63)$$

where we have again used that  $f$  is piecewise constant.

To conclude, we combine (54), (59), (60) and (63) to obtain that  $u_H \in V_H$  is the solution to

$$\begin{aligned} \forall v_H \in V_H, \quad \int_\Omega m \nabla u_H \cdot \nabla v_H + v_H b \cdot \nabla u_H + \tau^B (b \cdot \nabla u_H) (b \cdot \nabla v_H) \\ = \int_\Omega f v_H + \tau^B f b \cdot \nabla v_H. \end{aligned} \quad (64)$$

We exactly recognize the  $\mathbb{P}_1$  SUPG scheme (6). We conclude that the Adv-MsFEM-lin-B solution  $u_{H,B}^{\varepsilon, \text{adv}} \in V_{H,B}^{\varepsilon, \text{adv}}$  is given by (28), where the coarse scale component  $u_H \in V_H$  is the unique solution to the  $\mathbb{P}_1$  SUPG scheme (6) (with the stabilization parameter  $\tau^B$  given by (57)), and where  $\beta_K = f_K$ .

**Remark B.5.** The same effective scheme (64) for  $u_H$  is obtained for a variant of Adv-MsFEM-lin, without bubbles, that uses test functions  $\phi_i^{\varepsilon, \text{adv}, \star}$  solving the adjoint problem to (29), that is,

$$\forall K \in \mathcal{T}_H, \quad \begin{cases} \forall v \in H_0^1(K), \quad a_K^\varepsilon \left( v, \phi_i^{\varepsilon, \text{adv}, \star} \right) = 0, \\ \phi_i^{\varepsilon, \text{adv}, \star} = \phi_i^{\mathbb{P}_1} \quad \text{on } \partial K, \end{cases}$$

while still using  $V_H^{\varepsilon, \text{adv}}$  defined by (20) for the trial space. The effective scheme for  $u_H$  is not affected if bubble functions are added to the trial and test spaces.

## C Non-intrusive implementation of the Petrov-Galerkin Adv-MsFEM-CR variants

We detail here how to implement in a non-intrusive manner the Petrov-Galerkin variants introduced in Section 4.4. To that aim, we follow our exposition of [13, 12]. It is however worth noticing that we consider here variants including multiscale bubble functions, a feature not present in [13, 12]. We also note that our non-intrusive formulation eventually yields an effective equation where the right-hand side belongs to  $H^{-1}(\mathcal{T}_H)$  (and not  $L^2(\Omega)$ ), even if the right-hand side  $f$  of the equation of interest (1) belongs to  $L^2(\Omega)$ . The standard finite element code used to solve the effective problem must therefore be able to handle such terms. This is an additional requirement for the

finite element software that was not present in [12]. In passing, we note that we have corrected here a few erroneous calculations of [11].

To implement the PG Adv-MsFEM-CR approach (40) in a non-intrusive manner, we simply follow the general framework introduced in [12]. We begin by expanding the multiscale basis functions  $\phi_e^{\varepsilon,\text{adv}}$  (defined by (30)) in terms of the  $\mathbb{P}_1$  Crouzeix-Raviart basis functions  $\phi_e^{\mathbb{P}_1}$ , in a similar fashion as (23):

$$\phi_e^{\varepsilon,\text{adv}} = \phi_e^{\mathbb{P}_1} + \sum_{K \in \mathcal{T}_H} \sum_{\alpha=1}^d \partial_\alpha \left( \phi_e^{\mathbb{P}_1} \Big|_K \right) \chi_K^{\varepsilon,\text{adv},\alpha}. \quad (65)$$

For Adv-MsFEM-CR, the numerical correctors  $\chi_K^{\varepsilon,\text{adv},\alpha}$  ( $\alpha = 1, \dots, d$ ) are defined as the solution in  $H_{0,w}^1(K)$  to the problem  $a_K^\varepsilon \left( \chi_K^{\varepsilon,\text{adv},\alpha} + x^\alpha, v \right) = 0$  for all  $v \in H_{0,w}^1(K)$ .

The numerical correctors are used to define a piecewise constant diffusion matrix  $\bar{A}$  and a piecewise constant advection field  $\bar{b}$  as follows (see [12]):

$$\begin{aligned} \forall K \in \mathcal{T}_H, \quad \bar{A}_{\beta,\alpha} \Big|_K &= \frac{1}{|K|} a_K^\varepsilon \left( x^\alpha - x_{c,K}^\alpha + \chi_K^{\varepsilon,\text{adv},\alpha}, x^\beta - x_{c,K}^\beta \right), \quad 1 \leq \alpha, \beta \leq d, \\ \bar{b}_\alpha \Big|_K &= \frac{1}{|K|} a_K^\varepsilon \left( x^\alpha - x_{c,K}^\alpha + \chi_K^{\varepsilon,\text{adv},\alpha}, 1 \right), \quad 1 \leq \alpha \leq d, \end{aligned} \quad (66)$$

where  $x_{c,K} = (x_{c,K}^1, \dots, x_{c,K}^d)$  is the centroid of  $K$ . With these effective coefficients, we define the effective bilinear form

$$\forall u, v \in H^1(K), \quad \bar{a}_K(u, v) = \int_K \nabla v \cdot \bar{A} \nabla u + v \bar{b} \cdot \nabla u. \quad (67)$$

Denoting  $\mathbb{A}^{W,\mathbb{P}_1}$  the matrix of the linear system associated to the PG method (40), we have, for all interfaces  $e, h \in \mathcal{E}_H^{\text{in}}$ ,

$$\mathbb{A}_{h,e}^{W,\mathbb{P}_1} = \sum_{K \in \mathcal{T}_H} a_K^\varepsilon \left( \phi_e^{\varepsilon,\text{adv}}, \phi_h^{\mathbb{P}_1} \right) = \sum_{K \in \mathcal{T}_H} \bar{a}_K \left( \phi_e^{\mathbb{P}_1}, \phi_h^{\mathbb{P}_1} \right). \quad (68)$$

On the right-hand side of (68), we recognize the generic component of the matrix of the linear system associated to a standard  $\mathbb{P}_1$  Crouzeix-Raviart FEM that solves the following problem: find  $\bar{w}_H^{\varepsilon,\text{adv}} \in V_H^w$  such that

$$\forall v_H \in V_H^w, \quad \sum_{K \in \mathcal{T}_H} \bar{a}_K \left( \bar{w}_H^{\varepsilon,\text{adv}}, v_H \right) = F(v_H), \quad (69)$$

where the  $\mathbb{P}_1$  Crouzeix-Raviart  $V_H^w$  is defined by (41). Once the effective coefficients (66) have been computed, problem (69) can be solved by a standard Crouzeix-Raviart finite element solver.

Since the right-hand sides of the discrete problems (40) and (69) are identical (this is the interest of considering the Petrov-Galerkin formulation), and because of (68), the linear systems related to both problems are the same. We can thus compute the solution to (40) by solving (69) and expanding the solution of the linear system along the basis  $\left\{ \phi_e^{\varepsilon,\text{adv}} \right\}_{e \in \mathcal{E}_H^{\text{in}}}$  rather than  $\left\{ \phi_e^{\mathbb{P}_1} \right\}_{e \in \mathcal{E}_H^{\text{in}}}$ .

This is equivalent to setting

$$w_H^{\varepsilon,\text{adv},\text{PG}} = \bar{w}_H^{\varepsilon,\text{adv}} + \sum_{K \in \mathcal{T}_H} \sum_{\alpha=1}^d \partial_\alpha \left( \bar{w}_H^{\varepsilon,\text{adv}} \Big|_K \right) \chi_K^{\varepsilon,\text{adv},\alpha}, \quad \text{where } \bar{w}_H^{\varepsilon,\text{adv}} \text{ solves (69).}$$

The implementation is non-intrusive in the sense that only finite element problems based on standard  $\mathbb{P}_1$  elements (rather than multiscale finite element spaces) have to be solved.

We now turn to Adv-MsFEM-CR methods with bubbles. We can introduce a Petrov-Galerkin variant of either the Adv-MsFEM-CR-B (33) or the Adv-MsFEM-CR- $\beta$  (39b). For both methods, the coefficients for the bubble part can be computed element per element independently of the degrees of freedom in the space  $W_H^{\varepsilon, \text{adv}}$ , either according to (37) or as the local average of the right-hand side  $f$  in (39b). For a non-intrusive implementation of the MsFEM, one must avoid integrals of the product of  $f$  with highly oscillatory functions, since the numerical quadrature in a standard finite element software on the coarse mesh  $\mathcal{T}_H$  is not adapted to the approximation of such integrals. Such integrals appear in (37) but not in (39b). For these reasons, we have focused in Section 4.4 on a Petrov-Galerkin variant of the Adv-MsFEM-CR- $\beta$  method, which is (42).

The matrix of the linear system (42b) is exactly the matrix  $\mathbf{A}^{W, \mathbb{P}_1}$  from (68), which can thus be constructed in a non-intrusive fashion. It remains to find a formulation of the right-hand side of (42b) in terms of a  $\mathbb{P}_1$  scheme on the coarse mesh.

Fix a  $\mathbb{P}_1$  Crouzeix-Raviart function  $v_H \in V_H^w$ . Note that any such function satisfies, in all  $K \in \mathcal{T}_H$ ,

$$\forall x \in K, \quad v_H(x) = v_H(x_{c,K}) + \sum_{\alpha=1}^d \partial_{\alpha} (v_H|_K) (x^{\alpha} - x_{c,K}^{\alpha}), \quad (70)$$

because it is piecewise affine, where we recall that  $x_{c,K} = (x_{c,K}^1, \dots, x_{c,K}^d)$  denotes the centroid of  $K$ . Upon inserting this expression in the multiscale terms on the right-hand side of (42b), we obtain, for all  $K \in \mathcal{T}_H$ ,

$$a_K^{\varepsilon} \left( B_K^{\varepsilon, \text{adv}, w}, v_H \right) = v_H(x_{c,K}) a_K^{\varepsilon} \left( B_K^{\varepsilon, \text{adv}, w}, 1 \right) + \sum_{\alpha=1}^d \partial_{\alpha} (v_H|_K) a_K^{\varepsilon} \left( B_K^{\varepsilon, \text{adv}, w}, x^{\alpha} - x_{c,K}^{\alpha} \right).$$

We propose to compute in the offline stage of the MsFEM the piecewise constant quantities  $\mathcal{R}_0, \mathcal{R}_1, \dots, \mathcal{R}_d$  defined, on any  $K \in \mathcal{T}_H$ , by

$$\mathcal{R}_0|_K = \frac{1}{|K|} a_K^{\varepsilon} \left( B_K^{\varepsilon, \text{adv}, w}, 1 \right), \quad (71)$$

$$\mathcal{R}_{\alpha}|_K = \frac{1}{|K|} a_K^{\varepsilon} \left( B_K^{\varepsilon, \text{adv}, w}, x^{\alpha} - x_{c,K}^{\alpha} \right), \quad \alpha = 1, \dots, d. \quad (72)$$

This computation is similar to that of the effective diffusion coefficient and the effective advection field defined by (66). It then holds

$$\sum_{K \in \mathcal{T}_H} \beta_K a_K^{\varepsilon} \left( B_K^{\varepsilon, \text{adv}, w}, v_H \right) = \sum_{K \in \mathcal{T}_H} \beta_K |K| \left( \mathcal{R}_0|_K v_H(x_{c,K}) + \sum_{\alpha=1}^d \mathcal{R}_{\alpha}|_K \partial_{\alpha} (v_H|_K) \right),$$

where  $\beta_K = \frac{1}{|K|} \int_K f$ , and thus

$$\sum_{K \in \mathcal{T}_H} \beta_K a_K^{\varepsilon} \left( B_K^{\varepsilon, \text{adv}, w}, v_H \right) = \sum_{K \in \mathcal{T}_H} \beta_K \int_K \mathcal{R}_0 v_H + \mathcal{R} \cdot \nabla v_H, \quad (73)$$

where we have introduced the vector  $\mathcal{R} = (\mathcal{R}_1, \dots, \mathcal{R}_d)$ . Assuming that a standard finite element solver has a routine to compute the local averages  $\beta_K$  of the function  $f$ , all terms in (73) can be computed once the quantities  $\mathcal{R}_0, \dots, \mathcal{R}_d$  have been precomputed in the offline stage.



A non-intrusive formulation of the PG Adv-MsFEM-CR- $\beta$  method (42) can now be formulated as follows:

$$\text{Set } w_{H,\beta}^{\varepsilon,\text{adv,PG}} = \bar{w}_H^{\varepsilon,\text{adv,PG}} + \sum_{K \in \mathcal{T}_H} \sum_{\alpha=1}^d \partial_\alpha \left( \bar{w}_H^{\varepsilon,\text{adv,PG}} \Big|_K \right) \chi_K^{\varepsilon,\text{adv},\alpha} + \sum_{K \in \mathcal{T}_H} \beta_K B_K^{\varepsilon,\text{adv},w}, \quad (74a)$$

where  $\bar{w}_H^{\varepsilon,\text{adv,PG}} \in V_H^w$  solves

$$\forall v_H \in V_H^w, \quad \sum_{K \in \mathcal{T}_H} \bar{a}_K \left( \bar{w}_H^{\varepsilon,\text{adv,PG}}, v_H \right) = F(v_H) - \sum_{K \in \mathcal{T}_H} \beta_K \int_K \mathcal{R}_0 v_H + \mathcal{R} \cdot \nabla v_H, \quad (74b)$$

where  $\bar{a}_K$  is defined by (67). The latter problem no longer contains oscillatory coefficients and can be solved by a standard  $\mathbb{P}_1$  Crouzeix-Raviart finite element solver, provided terms of the form  $\sum_{K \in \mathcal{T}_H} \beta_K \int_K \mathcal{R} \cdot \nabla v_H$  (which corresponds to having a right-hand side in  $H^{-1}(\mathcal{T}_H)$ ) can be accommodated.

**Remark C.1.** Up to a slight modification, the Galerkin formulation (39) of Adv-MsFEM-CR- $\beta$  can also be implemented in a non-intrusive manner, thereby obtaining a formulation somewhat similar to (74). Using (65) and (70), we indeed obtain that

$$w_{H,\beta}^{\varepsilon,\text{adv}} = \bar{w}_H^{\varepsilon,\text{adv}} + \sum_{K \in \mathcal{T}_H} \sum_{\alpha=1}^d \partial_\alpha \left( \bar{w}_H^{\varepsilon,\text{adv}} \Big|_K \right) \chi_K^{\varepsilon,\text{adv},\alpha} + \sum_{K \in \mathcal{T}_H} \beta_K B_K^{\varepsilon,\text{adv},w},$$

where  $\bar{w}_H^{\varepsilon,\text{adv}} \in V_H^w$  solves

$$\forall v_H \in V_H^w, \quad \sum_{K \in \mathcal{T}_H} \bar{a}_K \left( \bar{w}_H^{\varepsilon,\text{adv}}, v_H \right) = F \left( v_H^{\varepsilon,\text{adv}} \right) - \sum_{K \in \mathcal{T}_H} \beta_K \int_K \mathcal{R}_0 v_H + \mathcal{R}^G \cdot \nabla v_H, \quad (75)$$

where  $\bar{a}_K$  is defined by (67),  $v_H$  and  $v_H^{\varepsilon,\text{adv}}$  are related by  $v_H^{\varepsilon,\text{adv}} = v_H + \sum_{K \in \mathcal{T}_H} \sum_{\alpha=1}^d \partial_\alpha (v_H|_K) \chi_K^{\varepsilon,\text{adv},\alpha}$  (see (65)),  $\mathcal{R}_0, \dots, \mathcal{R}_d$  are defined by (71)–(72) and  $\mathcal{R}_1^G, \dots, \mathcal{R}_d^G$  are defined by

$$\mathcal{R}_\alpha^G \Big|_K = \mathcal{R}_\alpha \Big|_K + \frac{1}{|K|} a_K^\varepsilon \left( B_K^{\varepsilon,\text{adv},w}, \chi_K^{\varepsilon,\text{adv},\alpha} \right), \quad \alpha = 1, \dots, d.$$

A non-intrusive implementation of (39) requires replacing  $F \left( v_H^{\varepsilon,\text{adv}} \right)$  by  $F(v_H)$  in (75). The resulting method is not equivalent to (39) and was found in our experiments to produce less accurate results than both the Galerkin variant (39) and the Petrov-Galerkin variant (42) of Adv-MsFEM-CR- $\beta$ . It is therefore not reported in this article.

## Acknowledgements

The first author acknowledges a PhD fellowship from DIM Math INNOV. The second and third authors are grateful to ONR and EOARD for their continuous support. The fourth author thanks Inria for the financial support enabling his two-year partial leave (2020-2022) that has significantly facilitated the collaboration on this project.

## References

- [1] A. Abdulle, W. E. B. Engquist, and E. Vanden-Eijnden. [The Heterogeneous Multiscale Method](#). *Acta Numerica*, 21:1–87, 2012.
- [2] A. Abdulle and M. E. Huber. [Discontinuous Galerkin Finite Element Heterogeneous Multiscale Method for advection–diffusion problems with multiple scales](#). *Numer. Math.*, 126(4):589–633, 2014.
- [3] G. Allaire and R. Brizzi. [A Multiscale Finite Element Method for numerical homogenization](#). *Multiscale Model. Simul.*, 4(3):790–812, 2005.
- [4] G. Allaire, S. Desroziers, G. Enchery, and F. Ouaki. [A Multiscale Finite Element Method for transport modeling](#). In *Proceedings of the 6th European Congress on Computational Methods in Applied Sciences and Engineering*, pages 3052–3069, Vienna, Austria, 2012.
- [5] D. N. G. Allen and R. V. Southwell. [Relaxation methods applied to determine the motion in two dimensions of a viscous fluid past a fixed cylinder](#). *Q. J. Mech. Appl. Math.*, 8(2):129–145, 1955.
- [6] R. Altmann, P. Henning, and D. Peterseim. [Numerical homogenization beyond scale separation](#). *Acta Numerica*, 30:1–86, 2021.
- [7] I. Babuška and J. E. Osborn. [Generalized Finite Element Methods: their performance and their relation to mixed methods](#). *SIAM J. Numer. Anal.*, 20(3):510–536, 1983.
- [8] C. Baiocchi and F. Brezzi. [Virtual bubbles and Galerkin-Least-Squares type methods \(Ga.L.S.\)](#) *Comput. Methods Appl. Mech. Eng.*, 105:125–141, 1993.
- [9] A. Bensoussan, J.-L. Lions, and G. Papanicolaou. [Asymptotic analysis for periodic structures. Reprint of the 1978 original with corrections and bibliographical additions](#). Providence, RI: AMS Chelsea Publishing, 2011.
- [10] R. A. Biezemans. MsFEM in FreeFEM: Release version 2.0.0, 2023. DOI: [10.5281/zenodo.8312014](https://doi.org/10.5281/zenodo.8312014).
- [11] R. A. Biezemans. [Multiscale problems: non-intrusive implementation, advection-dominated problems and related topics](#). PhD thesis, École des Ponts ParisTech, 2023. <https://pastel.hal.science/te1-04481733>.
- [12] R. A. Biezemans, C. Le Bris, F. Legoll, and A. Lozinski. [Non-intrusive implementation of a wide variety of Multiscale Finite Element Methods](#). *Comptes Rendus Mécanique*, 351(S1):135–180, 2023.
- [13] R. A. Biezemans, C. Le Bris, F. Legoll, and A. Lozinski. [Non-intrusive implementation of Multiscale Finite Element Methods: an illustrative example](#). *J. Comput. Physics*, 477:111914, 2023.
- [14] X. Blanc and C. Le Bris. [Homogenization theory for multiscale problems: an introduction](#), volume 21 of *MS&A (Modeling, Simulation and Applications)*. Springer, Cham, 2023.
- [15] F. Bonizzoni, P. Freese, and D. Peterseim. [Super-localized orthogonal decomposition for convection-dominated diffusion problems](#), 2022. arXiv preprint 2206.01975.
- [16] F. Brezzi, L. P. Franca, T. J. R. Hughes, and A. Russo.  [\$b = \int g\$](#) . *Comput. Methods Appl. Mech. Eng.*, 145:329–339, 1997.
- [17] F. Brezzi, D. Marini, and E. Suli. [Residual-free bubbles for advection-diffusion problems: the general error analysis](#). *Numer. Math.*, 85(1):31–47, 2000.
- [18] F. Brezzi and A. Russo. [Choosing bubbles for advection-diffusion problems](#). *Math. Models Methods Appl. Sci.*, 4(4):571–587, 1994.
- [19] A. N. Brooks and T. J. R. Hughes. [Streamline Upwind/Petrov-Galerkin formulations for convection dominated flow with particular emphasis on the incompressible Navier-Stokes equation](#). *Comput. Methods Appl. Mech. Eng.*, 32:199–259, 1982.
- [20] V. M. Calo, E. T. Chung, Y. Efendiev, and W. T. Leung. [Multiscale stabilization for convection-dominated diffusion in heterogeneous media](#). *Comput. Methods Appl. Mech. Eng.*, 304:359–377, 2016.
- [21] I. Christie, D. F. Griffiths, and A. R. Mitchell. [Finite Element Methods for second order differential equations with significant first derivatives](#). *Int. J. Numer. Meth. Eng.*, 10:1389–1396, 1976.
- [22] R. Codina, E. Oñate, and M. Cervera. [The intrinsic time for the Streamline Upwind/Petrov-Galerkin formulation using quadratic elements](#). *Comput. Methods Appl. Mech. Eng.*, 94(2):239–262, 1992.
- [23] P. Degond, A. Lozinski, B. P. Muljadi, and J. Narski. [Crouzeix-Raviart MsFEM with bubble functions for diffusion and advection-diffusion in perforated media](#). *Commun. Comput. Phys.*, 17(4):887–907, 2015.
- [24] A. K. Dond and T. Gudi. [Patch-wise local projection stabilized Finite Element Methods for convection-diffusion-reaction problems](#). *Numer. Methods Partial Differential Eq.*, 35(2):638–663, 2019.
- [25] J. Douglas and J. Wang. [An absolutely stabilized Finite Element Method for the Stokes problem](#). *Math. Comp.*, 52(186):495–508, 1989.

- [26] W. E and B. Engquist. [The Heterogeneous Multiscale Methods](#). *Comm. Math. Sci.*, 1(1):87–132, 2003.
- [27] Y. Efendiev, J. Galvis, and T. Y. Hou. [Generalized Multiscale Finite Element Methods \(GMsFEM\)](#). *J. Comput. Physics*, 251:116–135, 2013.
- [28] Y. Efendiev and T. Y. Hou. [Multiscale Finite Element Methods](#), volume 4 of *Surveys and Tutorials in the Applied Mathematical Sciences*. Springer New York, New York, NY, 2009.
- [29] D. Elfverson, V. Ginting, and P. Henning. [On multiscale methods in Petrov-Galerkin formulation](#). *Numer. Math.*, 131(4):643–682, 2015.
- [30] L. P. Franca, S. L. Frey, and T. J. R. Hughes. [Stabilized Finite Element Methods: I. Application to the advective-diffusive model](#). *Comput. Methods Appl. Mech. Eng.*, 95(2):253–276, 1992.
- [31] L. P. Franca, A. Nesliturk, and M. Stynes. [On the stability of residual-free bubbles for convection-diffusion problems and their approximation by a two-level Finite Element Method](#). *Comput. Methods Appl. Mech. Eng.*, 166(1-2):35–49, 1998.
- [32] L. P. Franca and A. Russo. [Deriving upwinding, mass lumping and selective reduced integration by residual-free bubbles](#). *Appl. Math. Lett.*, 9(5):83–88, 1996.
- [33] F. Hecht. [New development in FreeFem++](#). *J. Numer. Math.*, 20(3-4):251–265, 2012.
- [34] P. Henning and M. Ohlberger. [The Heterogeneous Multiscale Finite Element Method for advection-diffusion problems with rapidly oscillating coefficients and large expected drift](#). *Netw. Heterog. Media*, 5(4):711–744, 2010.
- [35] T. Y. Hou and P. Liu. [Optimal local multi-scale basis functions for linear elliptic equations with rough coefficients](#). *Discrete Contin. Dyn. Syst.*, 36(8):4451–4476, 2016.
- [36] T. Y. Hou and X.-H. Wu. [A Multiscale Finite Element Method for elliptic problems in composite materials and porous media](#). *J. Comput. Physics*, 134(1):169–189, 1997.
- [37] T. Y. Hou, X.-H. Wu, and Z. Cai. [Convergence of a Multiscale Finite Element Method for elliptic problems with rapidly oscillating coefficients](#). *Math. Comp.*, 68(227):913–944, 1999.
- [38] T. J. R. Hughes. [Multiscale phenomena: Green’s functions, the Dirichlet-to-Neumann formulation, subgrid scale models, bubbles and the origins of stabilized methods](#). *Comput. Methods Appl. Mech. Eng.*, 127(1-4):387–401, 1995.
- [39] T. J. R. Hughes, G. R. Feijóo, L. Mazzei, and J.-B. Quinicy. [The Variational Multiscale Method – a paradigm for computational mechanics](#). *Comput. Methods Appl. Mech. Eng.*, 166(1-2):3–24, 1998.
- [40] T. J. R. Hughes, L. P. Franca, and G. M. Hulbert. [A new Finite Element Method formulation for computational fluid dynamics: VIII. The Galerkin/Least-Squares method for advective-diffusive equations](#). *Comput. Methods Appl. Mech. Eng.*, 50:181–193, 1985.
- [41] T. J. R. Hughes, M. Mallet, and M. Akira. [A new Finite Element formulation for computational fluid dynamics: II. Beyond SUPG](#). *Comput. Methods Appl. Mech. Eng.*, 54(3):341–355, 1986.
- [42] G. Jankowiak and A. Lozinski. [Non-conforming Multiscale Finite Element Method for Stokes flows in heterogeneous media. Part II: error estimates for periodic microstructure](#). *Discrete Contin. Dyn. Syst. – Series B*, 29(5):2298–2332, 2024.
- [43] V. John and P. Knobloch. [On spurious oscillations at layers diminishing \(SOLD\) methods for convection–diffusion equations: Part I – A review](#). *Comput. Methods Appl. Mech. Eng.*, 196(17-20):2197–2215, 2007.
- [44] V. John, J. M. Maubach, and L. Tobiska. [Nonconforming streamline-diffusion-finite-element-methods for convection-diffusion problems](#). *Numer. Math.*, 78(2):165–188, 1997.
- [45] P. Knobloch and L. Tobiska. [The  \$P\_1^{mod}\$  element: a new nonconforming Finite Element for convection-diffusion problems](#). *SIAM J. Numer. Anal.*, 41(2):436–456, 2003.
- [46] C. Le Bris and F. Legoll. [Examples of computational approaches for elliptic, possibly multiscale PDEs with random inputs](#). *J. Comput. Physics*, 328:455–473, 2017.
- [47] C. Le Bris, F. Legoll, and A. Lozinski. [An MsFEM type approach for perforated domains](#). *Multiscale Model. Simul.*, 12(3):1046–1077, 2014.
- [48] C. Le Bris, F. Legoll, and A. Lozinski. [MsFEM à la Crouzeix-Raviart for highly oscillatory elliptic problems](#). *Chin. Ann. Math. Ser. B*, 34(1):113–138, 2013.
- [49] C. Le Bris, F. Legoll, and F. Madiot. [A numerical comparison of some Multiscale Finite Element approaches for advection-dominated problems in heterogeneous media](#). *ESAIM: Math. Model. Numer. Anal.*, 51(3):851–888, 2017.
- [50] C. Le Bris, F. Legoll, and F. Madiot. [Multiscale Finite Element Methods for advection-dominated problems in perforated domains](#). *Multiscale Model. Simul.*, 17(2):773–825, 2019.

- [51] C. Le Bris, F. Legoll, and F. Thomines. [Multiscale Finite Element approach for “weakly” random problems and related issues](#). *ESAIM: Math. Model. Numer. Anal.*, 48(3):815–858, 2014.
- [52] F. Legoll, P.-L. Rothé, C. Le Bris, and U. Hetmaniuk. [An MsFEM approach enriched using Legendre polynomials](#). *Multiscale Model. Simul.*, 20(2):798–834, 2022.
- [53] G. Li, D. Peterseim, and M. Schedensack. [Error analysis of a variational multiscale stabilization for convection-dominated diffusion equations in two dimensions](#). *IMA J. Numer. Anal.*, 38(3):1229–1253, 2018.
- [54] A. Målqvist and D. Peterseim. [Localization of elliptic multiscale problems](#). *Math. Comp.*, 83(290):2583–2603, 2014.
- [55] A. Målqvist and D. Peterseim. [Numerical homogenization by Localized Orthogonal Decomposition](#), volume 5 of *SIAM Spotlights*. Society for Industrial and Applied Mathematics, Philadelphia, PA, 2021.
- [56] B. P. Muljadi, J. Narski, A. Lozinski, and P. Degond. [Nonconforming Multiscale Finite Element Method for Stokes flows in heterogeneous media. Part I: Methodologies and numerical experiments](#). *Multiscale Model. Simul.*, 13(4):1146–1172, 2015.
- [57] P. J. Park. [Multiscale numerical methods for the singularly perturbed convection-diffusion equation](#). PhD thesis, Caltech, 2000. [https://thesis.library.caltech.edu/783/1/Park\\_pj\\_2000.pdf](https://thesis.library.caltech.edu/783/1/Park_pj_2000.pdf).
- [58] P. J. Park and T. Y. Hou. [Multiscale numerical methods for singularly perturbed convection-diffusion equations](#). *Int. J. Comput. Methods*, 01(01):17–65, 2004.
- [59] A. Quarteroni. [Numerical models for differential problems](#), volume 16 of *MS&A (Modeling, Simulation and Applications)*. Springer International Publishing, Cham, 3rd edition, 2017.
- [60] H.-G. Roos, M. Stynes, and L. Tobiska. [Robust numerical methods for singularly perturbed differential equations](#), volume 24 of *Springer Series in Computational Mathematics*. Springer Berlin Heidelberg, Berlin, Heidelberg, 2008.
- [61] Y.-Z. Su, S.-Y. Su, and F.-N. Hwang. [Locally adaptive bubble function enrichment for Multiscale Finite Element Methods: application to convection-diffusion problems](#). *Int. J. Numer. Meth. Fluids*, 95(10):1639–1655, 2023.